MAGNETIZATION DISCONTINUITIES AT MELTING AND FREEZING TRANSITIONS IN $YBa_2Cu_3O_{7-\delta}$

A.I. Rykov
Department of Applied Physics, The University of Tokyo, 7-3-1 Hongo, Bunkyo-ku, Tokyo 113-8656, Japan

I. INTRODUCTION

Considerable progress was recently made in understanding the rich and varied vortex phase behavior of high-T_c superconductors. The important role played by thermal fluctuations near T_c enriches the vortex phase diagram with a novel vortex liquid state. The liquid and solid phases are separated by the melting line $T_m(H)$ on which the thermal energy is strongly reduced compared to that on the mean-field line $T_{c2}(H)$. The melting line $T_m(H)$ appears to be the 1st order phase boundary located far below $T_{c2}(H)$ exactly as it was predicted for the thermal fluctuations in two dimensions $(D = 2)$ [1].

Recent experiments on the clean crystals of $Bi_2Sr_2CaCu_2O_8$ (BSCCO) and $YBa_2Cu_3O_{7-\delta}$ (YBCO) proved that the transition at the *low-field* branch of the T_m-line is indeed of 1st order [2-6]. Magnetization of a clean superconductor undergoes a jump at crossing the melting line. This was first demonstrated in BSCCO in which the melting line was traced by the (H,T)-location of the jump in the local magnetic induction [2]. In YBCO, the δ-spikes observed in specific heat $c_H(T)=\delta(T-T_m)$ leave no doubts [5] that the internal energy and entropy, associated with the vortex matter, changes discontinuously between the delineated aggregate states. The jumps in entropy ΔS and in magnetization ΔM are linked via Clapeyron-Clausius relation [6]:

$$\Delta S = - \mu_0 \Delta M \, (dH_m/dT_m) \qquad (1)$$

The evidences of jumps ΔS and ΔM are of fundamental importance for understanding the nature of the phase transition. In the liquid state, the entropy of vortex disordering is added to the entropy of vortex solid, however, a major contribution to ΔS near T_c comes from additional degrees of freedom related to divergence of penetration depth at $T \to T_c$ [7,8]. The sign of ΔM is that of densifying vortex matter at melting alike to the melting of ice into water. Most likely, the flux density increases at melting because the intervortex repulsion become screened with the addition of thermally excited vorticity[9]. On the other hand, for a high-fields branch of melting line $\Delta S = 0$.

***Fax** +81-0742-51-8005*

The transition in *high-fields* should be continuous as predicted in glass model [10] because the glassiness is favored by increasing vortex entanglement with increasing either disorder or anisotropy, which are both dual of rescaling the magnetic field. Therefore, the order of melting transition changes with increasing field. The line of 1st order transition terminates at a critical point (CP) to give a way to the line of the 2nd order transition [11,12].

In this paper, we observed the jumps ΔM in YBCO single crystals along the melting line on two sides of the CP. Concomitantly to the jumps, the λ–peaks appear in magnetization. Contrarily to the expectation (Eq.1), the jumps do not vanish above the CP, but show an apparent increase in magnitude. In lieu of narrow jumps, the magnetization shows the broad σ-like anomalies at crossing the melting line above CP. The transition widths differ by ~50 times between the λ-like 1st order and the σ-like 2nd order transitions. We investigate the irreversibility in a very close vicinity of the transition and show that the sharp transition below the CP exhibits the combined features for the 1st and 2nd order transitions. The admixture of the 2nd order character is related to the transient temporal behavior of magnetization. On the other hand, the purely 2nd order transition above the CP is of entirely different nature. Another phase transition line $H_{peak}(T)$, originating from the CP, goes inward the vortex solid and separates two solid phases which melts in the different ways. The location of the CP in the (H,T)-plane varies dramatically with slightly reducing oxygen content in YBCO crystals. The increase in δ up to optimal doping suppresses the CP down to zero-field. Therefore, the vortex solid in highly oxygenated YBCO melts abruptly within narrow temperature range, while the vortex solid in optimally doped YBCO melts continuously showing the broad σ-like curves M vs. T.

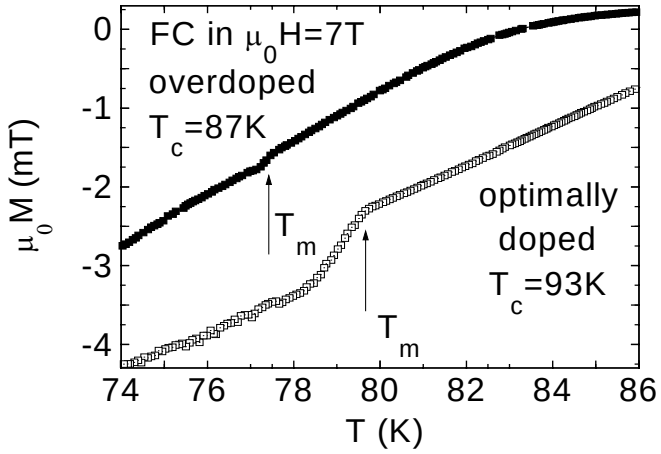

Fig.1. Magnetization $\mu_0 M$ vs. T for two different oxygen contents in the untwinned sample of $YBa_2Cu_3O_{7-\delta}$ measured in the field-cooled mode at warming (FCW) in the field of 7T . The jumps at T_m mark the transition for two doping levels in the same sample. According to Eq.1, only from the jump in the overdoped sample the vortex disordering entropy is within $1k_B$.

Figure 1 displays the bold manifestation of this result as measured with SQUID magnetometer in a 41-mg high-quality untwinned crystal of YBCO with dimensions 6 x 1.4 x 0.9 mm (L_axL_bxL_c). The details of measurements and sample preparation are given elsewhere [13,14]. The oxygen content in the sample was varied between "$O_{6.86}$" (optimally doped) and "O_7"(overdoped). The value of δ was ascribed to the sample according to the annealing temperature using the scale of Lindemer et al [15]. The data presented in the Sections I, II, III, V and VI were obtained for the field parallel to the c-axis. In Sec. VII, the magnetization discontinuities for the in-plane orientations of the field are studied. In Sec. II, we show the singularities in magnetization shaped as the inverse λ-peaks and discuss the interpretations of these features. We then turn to the magnetization observed at stepping the magnetic field in Sec.III. The theoretical expectations for the (T, H)-dependence of magnetization jumps are reviewed in Sec.IV and the attempts to describe them beyond the common models are sketched in Sec.VI. In Sec. V., the data for varying the oxygen deficiency δ are presented. In Sec. VIII, we look at some experimental artifacts. Sections IX and X present the discussion and the conclusions of the paper.

II. INVERSE λ-PEAKS OF MAGNETIZATION vs. TEMPERATURE

The first order transition implies that the temperatures of melting T_m and freezing T_f do not coincide. We have observed that the difference $\Delta T_{mf} = T_m - T_f$ indeed occurs clearly at crossing the *low-field* branch of the melting line. However, the non-zero quantity ΔT_{mf} is not the only manifestation of the irreversibility observed near the 1st order transition. The way by which the vortex state near the transition is obtained reveals itself in a few additional features of magnetization. Figure 2 shows the transition registered in a fully oxygenated YBCO crystal in a field cool cooling mode (FCC) in 7 Tesla. Contrarily to the FCW-magnetization of Fig.1, the FCC-magnetization shows a dip just below T_f. Subtraction of a smooth reversible magnetization M_s fitted for 2K above T_f leads to the reduced magnetization $M - M_s$ shaped as an inverse λ-peak. The excess of negative magnetization in the FCC mode characterizes the vortex state resulting from the freezing of the vortex liquid at $T_f \approx 77.3$ K.

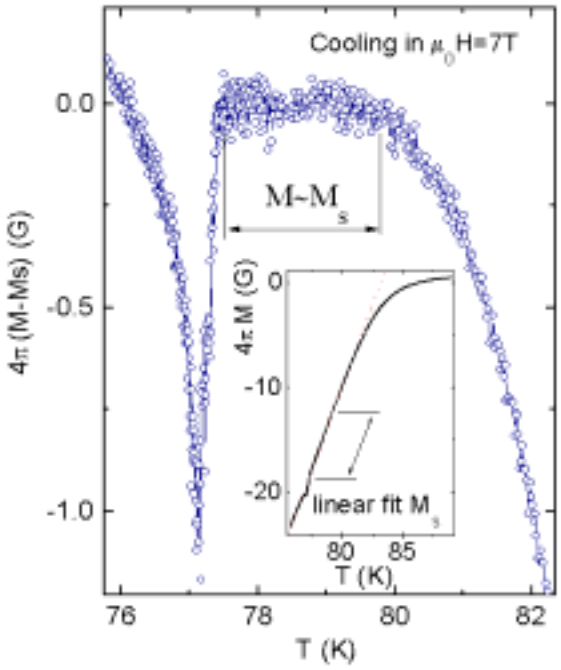

Fig.2. Inverse λ-peak of reduced magnetization at freezing transition in single crystal of $YBa_2Cu_3O_7$

Because the λ-peak is inverted, the freezing transition appears to induce the ejection of magnetic flux from the sample. The low-temperature shoulder of the λ-shaped magnetization would then indicate that a portion of magnetic flux reenters the sample as the temperature sweeps further below T_f. We have also tested this behavior in a different experiment, when the temperature sweep was stopped at T below T_m. The excess of negative magnetization was observed to relax with time at constant temperature. A recent interpretation of magnetization and entropy jumps [6], assumes that the melting/freezing transition occurs homogeneously only in a sample of an ellipsoidal shape. In this case, the intermediate state can be formed in which the solid fraction decreases gradually via melting.

On the other hand, the melting/freezing is not homogeneous in a rectangular sample. In this case, the intermediate state in one region of a sample coexists with the solid or liquid phases. The spatially localized phase boundary corresponds to a sheet of circular current flowing along the solid/liquid interface. A dip similar to that shown in Fig.2 appears already in the standard expression for the local density of magnetic flux near the current sheet in a long slab [6]. In the global magnetization, a dip was numerically observed as well. More complex structure involves a few oscillations of magnetization associated with the intermediate state within a few percent of H_{c1} near the dip [6].

The inhomogeneity of the vortex states in a real sample leads to the transient behavior reminiscent of 2nd order transition. In the case of rapid quenching, the system could be governed by a kinetic temperature, similar to that in 2nd order transition [16]. Observed in our experiment relaxation of the excess of the negative magnetization at constant T suggest a dissipation of the currents related to the interphase boundaries and topological defects. The relaxation is slowing down at freezing because the droplets of liquid phase can be trapped inside the solid phase. The nucleation of the vortex solid is

associated with enlarging a new order parameter (Φ-order [17]). During the growth of the nucleons, the orientation of the order parameter remains random in each nucleon. As the nucleons get in contact with each other, a tangle of singularities is formed similarly to the formation of vortices in ^{3}He [18,19]. Just below the transition the self-seeking character of the defect walks abruptly increases, so that the temperature dependence of the walk step shaped as an inverse λ-peak [20]. The dissipation of the interphase currents could be thus viewed as an annihilation of "matter and antimatter". The amplitude of the distribution of topological defects likewise exhibits an inverse λ-peak just below the transition [20].

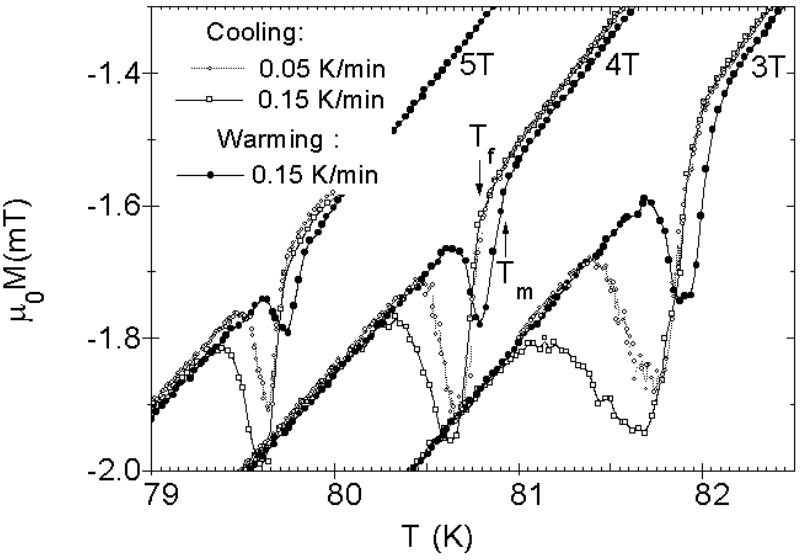

Fig.3. FCC magnetization measured in fields of 3, 4 and 5 Tesla with cooling rates of 0.05 K/min and 0.15 K/min and FCW magnetization measured at 0.15 K/min in a fully oxygenated YBCO single crystal. Note the temperature difference of 0.2K between melting and freezing. The temperatures T_m and T_f are not affected by the cooling/warming rate.

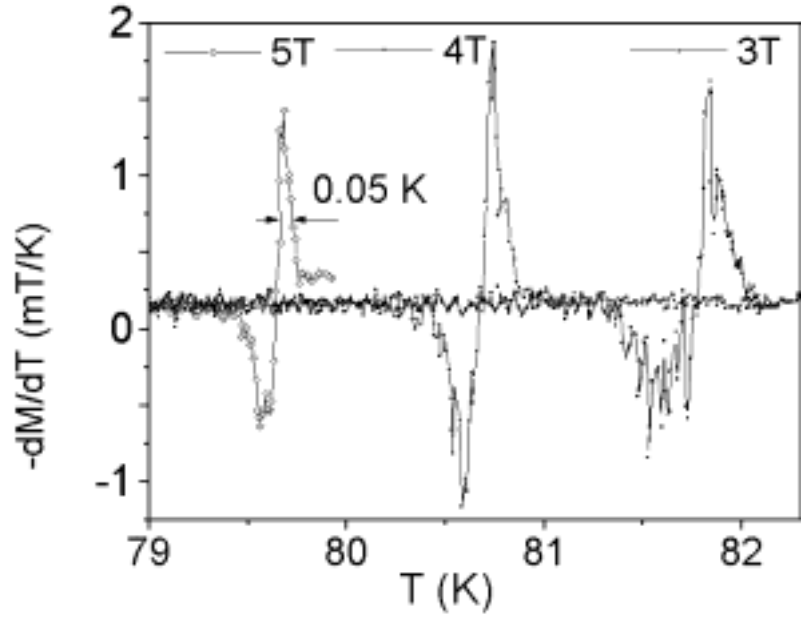

Fig.4. Temperature derivative $\mu_0 dM/dT$ of the slow field cool cooling (FCC, rate ~ 0.05 K/min) magnetization data of Fig.3. In the field of 5 Tesla, the freezing transition occurs over a width of 0.05 K. The transition width and the asymmetry of the inverse λ-peak increases with decreasing field.

Figure 3 shows that the inverse λ–peak shifts when the temperature sweep direction is reversed. The exact location of the upturn in the head of the inverse λ-peak depends also on the cooling rate. However, for increasing temperature all the sweeping rates in the range from 0.05 K/min to 2K/min gave the coinciding high-temperature shoulder of the inverse λ–peak. The inflection point where this shoulder adjoins the line of reversible magnetization is denoted as T_m. For decreasing temperature, all the sweeping rates gave another location of the high-temperature shoulder of the inverse λ–peak, which adjoins the line of reversible magnetization at T_f as shown in Fig.3. In the FCW-magnetization, the

inverse λ-peak shown in Fig.3 is an additional feature, which is not seen in Fig.1. It should be emphasized that this feature is observed only for the *low-field* branch of the melting line located below the CP. With a significant decrease of the oxygen content in the sample the CP goes to zero-field. This is the reason why this feature is not seen in the optimally doped sample of Fig. 1. On the other hand, this feature is present but not resolved for the overdoped sample of Fig.1.

The amplitude of the inverse λ-peaks for the FCW magnetization is systematically smaller than that for the FCC magnetization. With increasing field from 5T (Fig.3) to 7T (Fig.1) the FCW λ–peak becomes much tinier than the FCC-λ–peak. The ratio between these amplitudes is also sensitive to small variations in the oxygen content and the orientation of the sample. Figure 5 shows the FCW data of Fig.1 altogether with the FCC data measured in the same run. The physical picture of the 2nd order transition suggested above accounts for the difference between FCC and FCW magnetizations near T_m (T_f). In contrast, this difference cannot be explained by pinning. Figure 5 shows how we discern the ordinary pinning from the 2nd order transient behavior described above. The pinning is assessed by measuring the zero-field cooled (ZFCW) and reduced field warming (RFW) magnetizations. In the ZFCW procedure, the magnetic field is applied at low temperature where the critical current J_c is large, so that the Bean profile [21] is formed in the sample prior to the measurement. The RFW thermomagnetic protocol involves a precooling of sample in a field larger than the measurement field. An inverted Bean profile is formed when the field is reduced at low temperature.

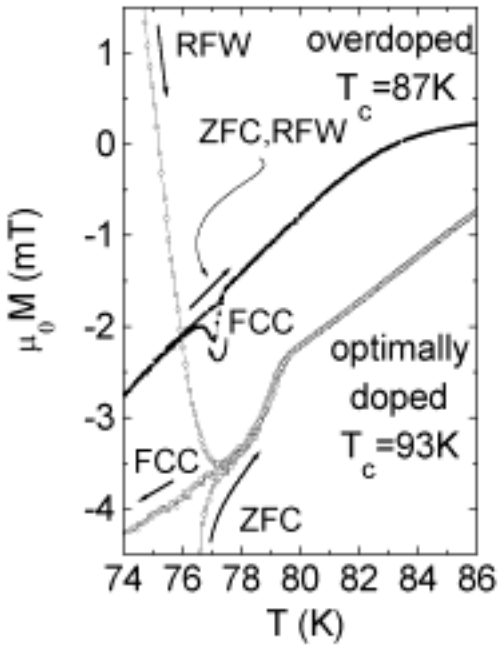

Fig.5. FCW and FCC magnetizations in the field of 7 T for two oxygen contents in the untwinned sample of $YBa_2Cu_3O_{7-\delta}$ The FCW data correspond to Fig.1. Also shown are the zero-field-cooling (ZFCW) data and the data obtained at warming sample in the field reduced (RFW) to 7T after cooling in a slightly larger field (~7.2T, obtained in the hysteresis mode of field setting into the SQUID magnet). In the optimally doped sample, the divergence between RFW and ZFCW data evidences an inversion of the Bean profile that is indicative of pinning ($J_c>0$). All the magnetizations obtained at warming in the overdoped sample (ZFCW, FCW, RFW) coincide far from T_m. This is in striking contrast in this sample with the FCC data showing the inverse λ–peak just below T_m.

Both RFW and ZFCW measurements are conducted at slow warming the sample. The straight and the inverted Bean profiles are steep at low temperatures, however, become shallower as the temperature approaches to T_m. In the optimally doped sample, the pinning persist right up till the σ-like anomaly, as indicated by the divergence of the ZFCW and RCW magnetizations. In the overdoped sample, the ZFCW and RFW magnetizations exactly coincide far below the transition. On the other hand, the splitting between the FCC and FCW magnetization branches near T_m occurs only in the overdoped sample. In the optimally doped sample, the fully coinciding FCC and FCW curves show no any mark of the inverse λ-peak. The transient phenomena mentioned above are not relevant to the purely 2nd order transition in the optimally doped sample. The freezing transition in the

optimally doped sample is instantly ensued by the onset of pinning just near the transition, it appears that the pinning suppress the vortex state, associated with the inverse λ-peak.

Figure 6 shows the magnetization measured in the overdoped sample for a number of fields H_{app} for temperature sweeps up (ZFCW, RFW) and down (FCC). The cooling/warming rate is larger than that in Fig.3. As in Fig.5, the ZFCW and RFW data in 7T fully coincide both above and below the transition, showing that the pinning is negligible in this field. As the field decreases, a divergence between the cooling data (FCC) and warming data (ZFCW, RFW) start to appear below the transition. On the other hand, in the immediate vicinity of transition, this discrepancy decreases. In the field of 3T, the magnitude of the inverse λ-peak is nearly the same in the cooling and warming data. Starting from the field of 3T, a difference between ZFCW data and RFW data is seen right up to the transition. In the field of 2T, the jump in ZFCW magnetization exceeds twice the jump in FCC magnetization, while the latter is yet twice larger than the jump in RFW magnetization. Clearly, the pinning in this field is robust right up to the transition.

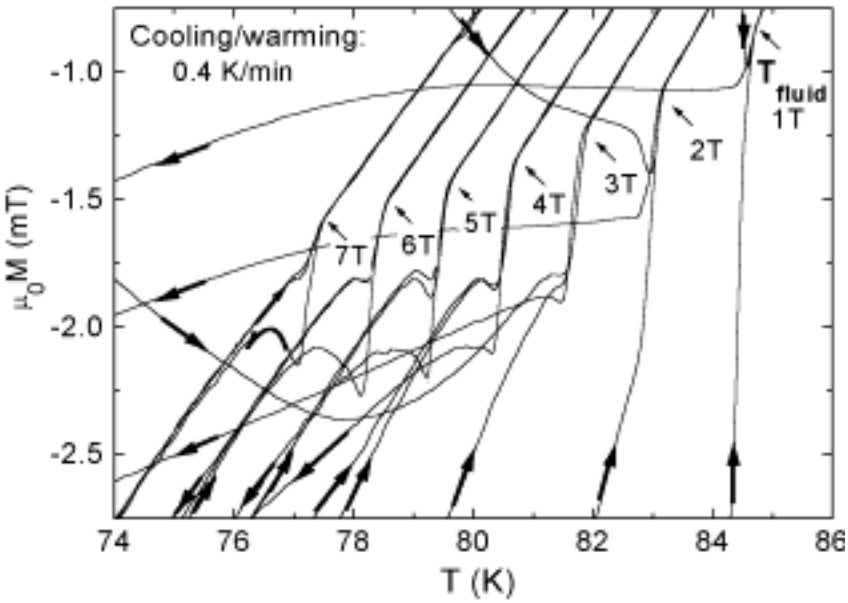

Fig.6. The $\mu_0 M$ vs. T curves in fields H_{app} of 1, 2, 3, 4, 5, 6 and 7 Tesla obtained according to three thermomagnetic protocols: ZFCW, FCC, and RFW. The thick arrows on the curves indicate increasing T for ZFCW and RFW modes and decreasing T for FCC mode. All the curves are coinciding above the onset of fully reversible state at T_{fluid} indicated for each value of H_{app}.

It was noted above that pinning suppress the transient vortex state associated with the inverse λ-peak. This was evident in the optimally doped sample. It follows from the Fig.6 that a similar suppression of the transient vortex state occurs in the overdoped sample for the low-field regime only. From Fig.7 it is also clear how the pinning affects the FC-magnetization. Both the FCC and FCW branches of FC magnetization in the low-field regime are shown in Fig.7. The slope of the FCC magnetization below the jump is smaller than the slope of reversible magnetization. As the temperature decreases, the pinning sets in below the jump. The Bean profile is gradually formed and the gradient of flux density increases with decreasing temperature. From thermodynamical reasoning for $J_c=0$ one expects the FCC magnetization below the jump closely following the slope of reversible magnetization. However, J_c increases continuously with decreasing temperature thereby reducing dM/dT. When the Bean profile is formed, only surface density of magnetic flux is in equilibrium with the external field. However, if the flux density is allowed to relax for a large time, one expects that the slopes of FC magnetization below the jump and above the jump equalize. The ordinary creep of magnetic flux is thus at the origin of difference between the FCC and FCW magnetizations in this case.

Thus, the appearance of pinning for low fields in the overdoped sample and for all fields in the optimally doped sample allowed us to explain the behavior of magnetization measured with using different thermomagnetic protocols. On the other hand, the transient

behavior of magnetization near the jump that appears in the high-field regime of the overdoped sample cannot be justified in terms of pinning. The plausible physical picture in which the inverted λ-peaks are associated with vortex loops is proposed.

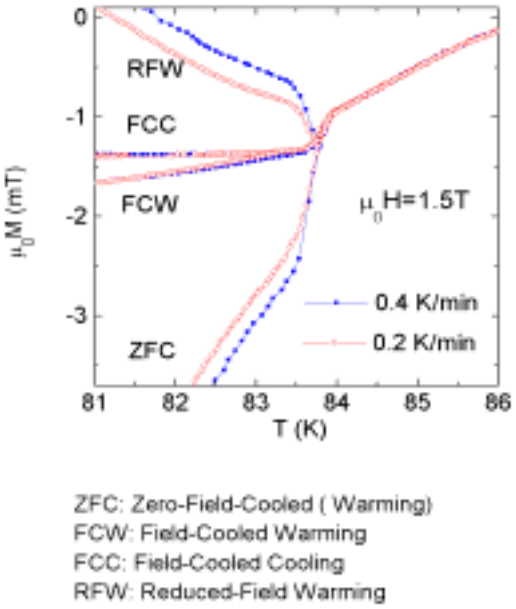

ZFC: Zero-Field-Cooled (Warming)
FCW: Field-Cooled Warming
FCC: Field-Cooled Cooling
RFW: Reduced-Field Warming

Fig. 7. ZFCW, FCW, FCC and RFW magnetizations in the field of 1.5 T for two rates of temperature sweep in the untwinned overdoped sample of $YBa_2Cu_3O_{7-\delta}$. The effect of the temperature sweep rate on the ZFCW and RFW magnetizations is indicative of the creep of magnetic flux.

It is worth to note that magnetization calculated in a frustrated 3D XY model [9] experience at the transition a change of about 7 to15%, comparable to that in Fig.3. This change in the vortex density was interpreted to take place as a consequence of the screening of repulsive intervortex interactions by the thermally excited vortex loops [9]. While the magnetization jump always manifest itself in the uniformly frustrated model, the entropy change becomes eventually so broad that can be hardly observed numerically. In the vortex lattice, the vortices are well aligned and the interactions between them are purely repulsive. In the vortex liquid, the interactions, which are proportional to the cosine of the angle between the vortex lines, may become attractive. Therefore, it is conjectured [9] that the jump in the vortex density, may not coincide with the melting of lattice, but correspond to a development of an infinite vortex tangle at a temperature T_l. In practice, the temperatures T_m, T_f, and T_l lie very close to each other; a small differential between them could be at the origin of the magnetization curve imitating a λ-shaped derivative.

The main result of this Section and a foresight for the results of the next Section should be brought together as follows. The inverse λ-peaks are observed only at crossing the melting line for $T>T_{CP}$. No fishtails exist in the $M-H$ loops for this field region. There occurs a correspondence between the shape of the $M-T$ curves and the $M-H$ loops:

(I) No classical broad fishtails occurs in the M-H curves above T_{CP}. In the region of fields $H<H_{CP}$, the $M-T$ curves are shaped as inverted λ-peaks; FCC and FCW curves diverge.

(II) The standard broad fishtails occur below T_{CP}. In the region of fields $H>H_{CP}$, the $M-T$ curves shows the broad σ-like anomalies, which are reversible; FCC and FCW curves are fully coinciding. This is found for various oxygen contents, which control the location of the CP as shown in Sec. V. In the next Section, the $M-H$ loops are assessed.

III. MAGNETIZATION JUMPS AT CLOSING THE M-H LOOPS

The combined effect of creep and flow of magnetic flux below T_m makes the hysteresis loops dependent on the field step ΔH employed in the discontinuous measurement with SQUID magnetometer. Shown in Fig.8 are the magnetization curves M_i vs. H_i measured in such a mode that the prolonged relaxation of magnetic flux at each field $H_i = i\Delta H$ was avoided. The onset of irreversibility observed in this condition does not depend on ΔH. The irreversibility appears at the same $H_m(T)$-line as in the temperature-sweep measurements. The inflection point where the second derivative of $M(H)$ curve takes the minimum defines the field H_m here. A premelting peak occurs at a field smaller than H_m by about 2 kOe. The exact field location of the premelting peak barely changes with changing ΔH. Therefore, the interval between H_{peak} and H_m changes only a little with changing ΔH. On the other hand, the magnetization itself depends dramatically on ΔH.

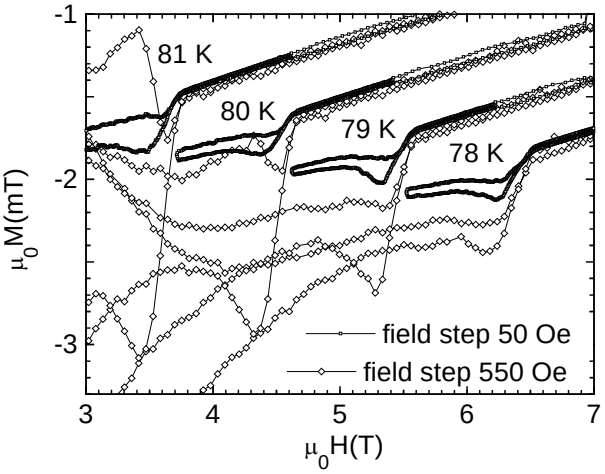

Fig.8. M vs H obtained in overdoped $YBa_2Cu_3O_7$ sample by stepping the applied field with ΔH of ±50 Oe and ±550 Oe.

The main effect at low temperature, for example, 78 K, consist of a uniform shift of both forward and reverse legs of the hysteresis loop. On the other hand, at higher temperature, e.g. 81 K, the splitting between the forward and reverse legs increases with increasing ΔH . These differences in M vs.H curves near transition should be associated with the differences observed in the M vs. T curves along the melting line. When the pinning and creep extends right up the transition as discussed in the previous Section, the splitting between forward and reverse legs strongly depend on ΔH . On the other hand, when the M-T curves exhibit the inverse λ-peaks, strongly dependent on the cooling rate, the main effect of ΔH on the M vs H curves consist of the uniform shift of the magnetization level below the transition.

The electric field that is produced upon stepping the magnetic field is proportional approximately to $\Delta H/\Delta t$, where Δt is time of setting the field H_i . Because Δt is not significantly changed in the experiment, the electric field increases proportionally to ΔH. The supercurrent induced in the sample and evaluated by the magnitude of splitting between the forward and the reverse legs of M increases with increasing the electric field.

Figure 9 illustrates the increase of the J_c level just near H_m with increasing T. This increase is closely related to the origin of zero-field peak of J_c. The J_c falloff with increasing field is quick, close to exponential. On the other hand, both the temperature dependence of H_m and the temperature decay of magnitude of zero-field peak are algebraic.

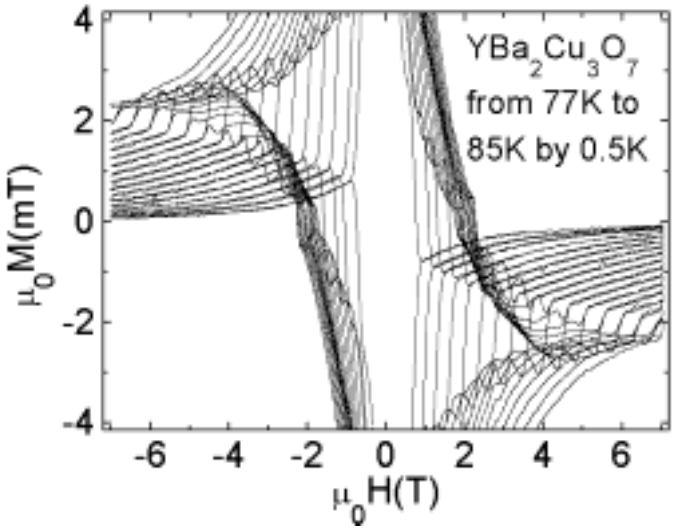

Fig.9. *M-H* hysteresis loops obtained in $YBa_2Cu_3O_7$ between 77K and 85K with $\Delta H = \pm 550$ Oe.

The region of critical fluctuation cover the region of zero-field peak of critical current near T_c. Therefore, we plotted the irreversible magnetization against $H/t^{2\nu}$ in Fig.10. In the fully oxygenated sample, the value of H_m at 77.4 K is ≈7 Tesla (Fig.9). The perfect oxygenation in the pulling-grown crystals leads to the strong reduction of T_c from the maximum value of 93.5 K. The minimum value of T_c on the overdoped side, which corresponds to the sample of Fig.9 is 86.7 K. Combining from T_m, H_m and T_c the 3D XY variable $\mu_0 H^* = \mu_0 H_m/(1-T_m/T_c)^{1.338}$ [22] we get 139 Tesla. This is the melting field extrapolated to zero T. When M is plotted against the variable $\mu_0 H/(1-T/T_c)^{1.338}$, the hysteresis loops are closing at 139 Tesla for arbitrary T in the range of 3D XY scaling. It is shown for this sample in Fig.10 (d) that all the M-H curves are also collapsed into a single universal hysteresis loop, except the region of fishtail. For the other contents of oxygen in the sample, the hysteresis loops are closing at $\mu_0 H^*$ smaller than 139 T. For "$O_{6.86}$" $\mu_0 H^*$ is only 34 Tesla (Fig.10 (a)). The zero-field peak plotted against $\mu_0 H/(1-T/T_c)^{1.338}$ is scaled into the iniversal curve for all the samples with different oxygen content.

The scaling of the data near zero-field in Fig.10 can be presented approximately as

$$J_c(H,T) = J_c(0,0)\, t^{2\nu}\, e^{-H/(H_0^*(t^*)^{2\nu})} \qquad (2)$$

with $t = t^* = 1-T/T_c$ and $\mu_0 H_0^* = 0.6$T independent of oxygen content. It is assumed in the scaling of Eq.2 that the field dependence of J_c near the zero-field peak is exponential: $J_c = J_c(0,T)e^{-H/H_0(T)}$. The Eq.(2) describes in average the change of J_c in a broad (T,H)- range (Fig.10). However, due to the rapid decrease of J_c with field, that is exponential only approximately, the value of J_c just below the transition is not described by the Eq.(2). When $t=t^*$, $J_c(H_m)$ should increase slowly with decreasing temperature. In Fig.9, the value of J_c just below the melting transition decreases with increasing H_m. It is likely that a reason for this discrepancy is in a small difference between the arguments $t = 1-T/T_c$ and $t^* = 1-T/T^*_c$ for the melting line $H_m(T)=H^* t^{2\nu}$ and the zero-field peak width $H_0(T)=H_0^*(t^*)^{2\nu}$. This result correspond to a phase diagram with different mean-field T_c^* and the true T_c of superconducting transition [17].

It is worth to mention the different nature of premelting peaks (Fig.9) and the fishtails (Fig.10). The fishtails which appear near T_c in samples with relative low oxygen content (Fig.10 (a),(b)) are located at nearly half of H^*, while the premelting peaks is located above $0.95H_m$ as shown in Fig. 9. In the sample with the highest oxygen content of Fig.10, these small premelting peaks should reside notably far ($0.95H^*$~133T). In the samples "$O_{6.91}$" (Fig.10(c)) and "$O_{6.99}$" (Fig.10(d)), the curves M *vs.* H shown for lowest

temperatures of 75K (Fig.10 (c)) and 50 K (Fig.10 (d)) exhibit the onset of fishtails, indicating that the CP's are located above these temperatures. The field location of the CP's H_{CP} decreases with decreasing the oxygen content, so that the CP's fall into the measurable range of H (≤7T) in Fig.10 (a) and (b). The rise of fishtails below T_{CP} is due to the vortex entanglement associated with the pointlike disorder [23].

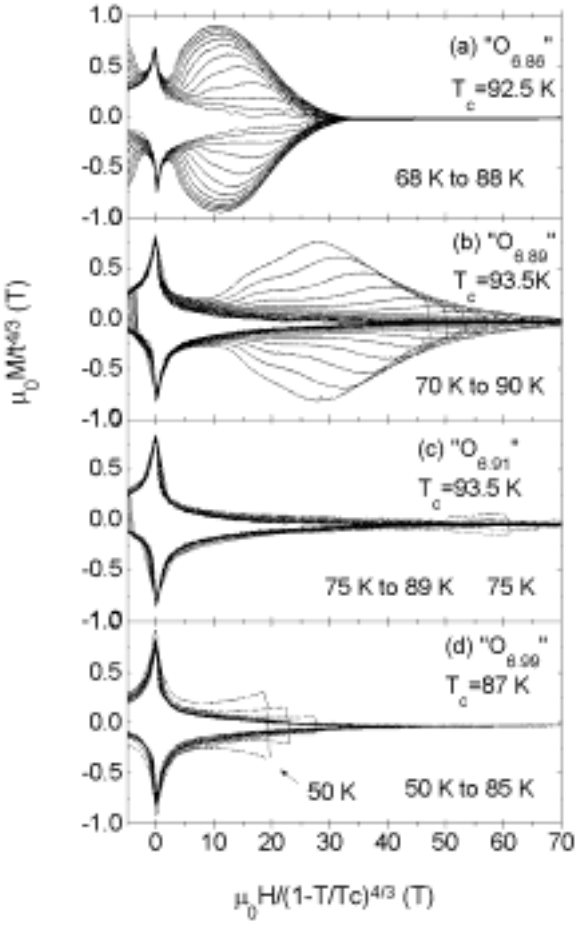

Fig. 10. Magnetization hysteresis loops scaled in coordinates $\mu_0 M/t^{4/3}$ vs. $\mu_0 H/t^{4/3}$ for the sample oxygenantions "$O_{6.86}$"(a), "$O_{6.89}$"(b), "$O_{6.91}$"(c) and "$O_{6.99}$"(d).

In the broad temperature range of fishtail absence in Fig.10 (c) and (d), the pointlike disorder is not significant. On the other hand, the pointlike disorder become important with decreasing temperature. The critical point delineate this regime at $T^{(1)}$ $(=T_{CP})$. With further decreasing temperature, the role of thermal fluctuations gradually decreases. In the low T regime, the transition is dominated by the pointlike disorder alone. According to cage model [24], in the limit of low T, the field-driven "disorder-induced" plastic transition is temperature independent, $H_{pl}^{dis}=H_{pl}^{dis}(0)$. The low-$T$ regime is defined by the single vortex depinning temperature T^*. In the intermediate region, the transition line is determined by both the pointlike disorder and the thermal fluctuations. In this regime, $T^*<T<T^{(1)}$, the field of plastic transition was shown theoretically[23,24] and identified experimentally[25] to increase with temperature:

$$H_{pl}^{dis}=H_{pl}^{dis}(0)(T^*/T)^{3.33}\exp[(2c/3)(T/T^*)^3] \qquad (3)$$

In Eq.3, c is the the constant of the order of unity[24]. The transition field H_{pl}^{dis} increases with increasing T because the disorder potential is flattened by thermal fluctuations.

The H_{pl}^{dis} in highly oxygenated YBCO crystals was identified in Ref. [25] with the beginning of the abrupt increase of J_c at the onset of the anomalous peak effect.

Recently the origin of the anomalous premelting peaks in $CeRu_2$ and 2H-$NbSe_2$ was examined [26] and attributed to "disorder-induced fracturing and entanglement of the vortex lattice". The location of premelting peak in these materials quite near the irreversibility line, $H_{peak} \sim 0.9 H_{irr}$, is similar to that shown in our Figs. 8 and 9. In our data, only 2kOe separate the H_{peak} from H_{irr}. In the cage model [24], the high-temperature branch of the melting line for $T > T^{(1)}$ is not influenced by the point disorder. Also in the 3D XY model [22], the line of melting transition $H_m = H^*/(1-T/T_c)^{1.338}$ is essentially the mean-field line $H_{c2}(T)$ suppressed merely by thermal fluctuations, $H_m = C H_{c2}$ (C=Const). According to theory[24], above $T^{(1)} = T_{CP}$, the point disorder potential is fully smeared out by the thermal fluctuations. The onset of the anomalous peak at the thermally induced plastic transition $H_{pl}^{th} = H_{peak}$ is at $0.95 H_m(T)$ in Fig.9.

In 2H-$NbSe_2$, the onset of the anomalous peak effect is hysteretic, as observed in resistivity[27]. The low-field edge of irreversibility at the onset of the peak is shifted as the direction of field sweep is reversed. The onset of peak effect is also attributed in Ref.[27] to the vortex lattice disordering. The ordering/disordering transition occurs at H_{pl}^{up} and H_{pl}^{down}, where the indexes "up" and "down" refer to the direction of field sweep. It is believed that the difference in population of topological defects between upward and downward sweeps is at the origin of the difference between H_{pl}^{up} and H_{pl}^{down} [27]. On the other hand, the interpretation of difference between the curves for H^{up} and H^{down} in our Fig.8 is not unequivocal. The ambiguity comes from the possibility of changing the magnetic moment in the course of measurement in the SQUID magnetometer [13]. Beside the transition-related changes of M, such as jump for the 1st order component and a λ-peak for the concomitant 2nd order component, the magnetic moment changes because of the decay of the electric field generated at setting the H-field. This decay is relevant to the data shown in Fig.8, because we avoided the long flux relaxation prior to measurement. Furthermore, Ravikumar et al [28,29] have pointed out that when the magnetization has an irreversible part, a large error in the reverse leg of the hysteresis loop can be caused by the effect of field inhomogeneity on the value of J_c. The premelting peak was also interpreted to come from a few twin boundaries residing in the sample[30]. Such a interpretation cannot be ruled out unequivocally because a small number of residual thin twining stripes occur also in our crystals, by virtue of their large size. It can be argued, however, that the premelting peak is intrinsic for untwinned YBCO. First of all, we observe this peak in other field orientations. Second, this premelting "bubble" was observed recently by torque magnetometry in a tiny untwinned crystal [31]. This method, free of the influence of inhomogeneous field, shows also that the "bubble" grows with increasing the sweeping rate. Finally, one more argument for the intrinsic nature of the "bubble" in YBCO is given by the similarity of the premelting peak in YBCO to that in $CeRu_2$ and 2H-$NbSe_2$.

Recent torque measurements in a high-quality untwinned YBCO-crystal [31] showed that the irreversibility persists right up to the melting transition. In practice, the separation of the hysteretic magnetization from the magnetization jumps is difficult. The incidental suppression of irreversibility is caused by the various quakes during a measurement. The vortex shaking process extends dramatically the reversible region in the phase diagram [32,33]. A fast relaxation also can hide a nascent irreversibility. The scenario elaborated in Refs. [28,29] suggest that the suppression of irreversibility can result in the M-H curves reminiscent of the jumps at the 1st order transition. The separation between the jumps and the premelting peaks requires a scrupulous handling. To proceed to the experimental details on field and temperature dependence of the magnetization jumps in Sect. V, it is useful to consider first the jumps in the theory of linelike melting (Sec.IV).

IV. (T,H)-DEPENDENCE OF MAGNETIZATION JUMPS AND LATENT HEAT

From the very general grounds of flux-line structure description, to maintain the Abrikosov crystalline lattice, the distance between vortices a_0 should be kept much larger than the thermal root mean squared displacement of the vortices $\langle u^2\rangle^{1/2}$. The Lindemann number c_L links these quantities at the event of melting. The melting transition is relevant to the phase diagram of a system of interacting elastic lines. Lindemann criterion predicts melting to occur when the root mean squared displacement exceed a fifteenth of a center-to-center nearest neighbor distance in a crystal, $c_L>0.15$. The intensity of vortex motion which gives rise to $\langle u^2\rangle$ is the function of anisotropy $\varepsilon=(m/M)^{1/2}$, the penetration depth $\lambda(T)$ and flux quantum Φ_0. At melting this function is equated to thermal energy $k_BT_m=(4\pi)^{-3/2}\ c_L^2\,\varepsilon\,a_0\ \Phi_0^2/\lambda^2$ [34]. With $a_0=(\Phi_0/B)^{1/2}$ the general expression for the melting line becomes:

$$B_m=\frac{c_L^4\varepsilon^2\Phi_0^5}{(4\pi)^3\lambda^4(k_BT_m)^2} \tag{4}$$

The derivative dB_m/dT can be substituted into the Clapeyron-Clausius relation (Eq.1) in place of $\mu_0\,dH_m/dT$ using the approximation $B_m\approx\mu_0H_m$, which is precise in YBCO. This allows to rewrite Eq.1 as follows:

$$\Delta S=2\Delta MB_m(1+2T_m\lambda^{-1}\ d\lambda/dT_m)/T_m \tag{5}$$

Due to the temperature dependence of λ, the entropy jump ΔS is strongly enhanced as T approaches to T_c along the melting line. Integrating the Eq. (5) over the elementary pancake volume $d\Phi_0/B_m$ gives Clapeyron-Clausius equation for the entropy per vortex per Cu_2O_4 layer ($d=0.117\ nm$):

$$\Delta S_d=2\Delta M\ d\Phi_0(1+2T_m\lambda^{-1}\ d\lambda/dT_m)/T_m \tag{6}$$

The latent heat per vortex per bilayer $Q_d=\Delta S_dT_m$ can be regarded as a sum of two terms:

$$Q_d=Q_{0d}+Q_{0d}\,2T_m\lambda^{-1}\ d\lambda/dT_m \tag{7}$$

where

$$Q_{0d}=2\Delta Md\Phi_0 \tag{8}$$

is the rather small latent heat obtained in Monte-Carlo simulations with a typical value of $0.07k_BT_m$ [35]. Typical experimental values of Q_d exceed Q_{0d} by an order of magnitude. While Q_d is determined exclusively by the field-induced vortices, the second term in Eq.(7) takes into account the microscopic degrees of freedom underlying the temperature dependence of the London penetration depth $\lambda(T)$. The latter leads to the enhancement of the total entropy ΔS with respect to its configurational part ΔS_0, as suggested by Dodgson et al [8]. The interpretation of the temperature dependence of the free energy within the London model in Refs.[7,8] renders precisely :

$$\begin{aligned}\Delta S&=\Delta S_0\ (1+2T\lambda^{-1}\,d\lambda/dT)\\ \Delta S_d&=\Delta S_{0d}\ (1+2T\lambda^{-1}\ d\lambda/dT)\end{aligned} \tag{9}$$

where $\Delta S_{0d}=2\Delta M d\Phi_0/T_m=Q/T_m$. It is conceivable to link the first and the second terms of the factor $1+2T\lambda^{-1}d\lambda/dT$ with the rearrangement in the field-induced and in the thermally generated degrees of freedom, respectively. The thermally generated degrees of freedom are the electronic degrees of freedom associated with the fluctuations of the amplitude of the superconducting order parameter.

Considering the procedure of the field-induced vortex disordering at melting, Dodgson et al [8] have expressed the configurational term ΔS_0 through the number of the elementary degrees of freedom $N_{edf} = 1/\varepsilon a^3_0 = (B/\Phi_0)^{3/2}/\varepsilon$:

$$\Delta S_0 = \eta k_B (B_m/\Phi_0)^{3/2}/\varepsilon$$
$$\Delta S_{0d}=\eta d k_B (B_m/\Phi_0)^{1/2}/\varepsilon \qquad (10)$$

so that each degree of freedom contribute to ΔS_0 with a small fraction of k_B, namely:

$$\eta k_B=(2\pi)^{-1} k_B \qquad (11)$$

Temperature dependence of the magnetization jumps can be obtained expressing ΔM either from Eq.(5) or from Eq.(6) and substituting the configurational part of entropy from Eqs.(10), with Eqs.(9) taken into account:

$$\Delta M= \eta k_B T_m B_m^{1/2} /2 \varepsilon\Phi_0^{3/2} \qquad (12)$$

Substituting B_m from Eq.(4) and η from Eq.(11) into Eq.(12) leads to

$$\Delta M = \frac{c_L^2 \Phi_0}{(4\pi)^{5/2}\lambda^2} \qquad (13)$$

Using this result, the Eq.(8) is rewritten as follows:

$$Q_{0d} = \pi^{-1/2} d c_L^2 (\Phi_0/4\pi\lambda)^2 \qquad (14)$$

Choosing $c_L = 0.15$ gives to the following estimate for the jump of magnetic induction

$$\Delta B=\mu_0\Delta M= 4.0 \times 10^{-5} \mu_0\Phi_0/\lambda^2 \qquad (15)$$

Converting this to CGS units ($\Phi_0 = 2.07\times10^{-6}$ G/cm^2) , gives $\Delta B=5.1\times10^{-4} \Phi_0/\lambda^2$. This result was obtained also in Ref. [36]. The temperature dependence of ΔM $(\sim\lambda^{-2})$ follows that of Q_{0d}, the latent heat obtained in the Monte-Carlo simulations. We see thus that ΔM should vanish monotonously with T approaching to T_c. The experimental results, described in the next section, shows that the apparent magnetization jumps (inverse λ-peaks) are not monotonous. Indeed, the magnetization jumps ΔM should vanish not only at $T \rightarrow T_c$ but also at $T\rightarrow T_{CP}$, because the 1st order transition character vanish at the CP. Most frequently, the jumps ΔM culminate at the fields intermediate between the lower and upper critical points. The sources of the nonmonotonousness of $\Delta M(H,T)$ are also discussed in the Sections VI and IX.

V. DIFFERENT OXYGEN CONTENTS IN YBCO

The behavior of magnetization in a vicinity of melting transition depends dramatically on the sample oxygenation. The plots of both the full and the reduced magnetization indicate in general that the inverse λ-peaks increase in magnitude and in width with desoxygenation (Fig.11).

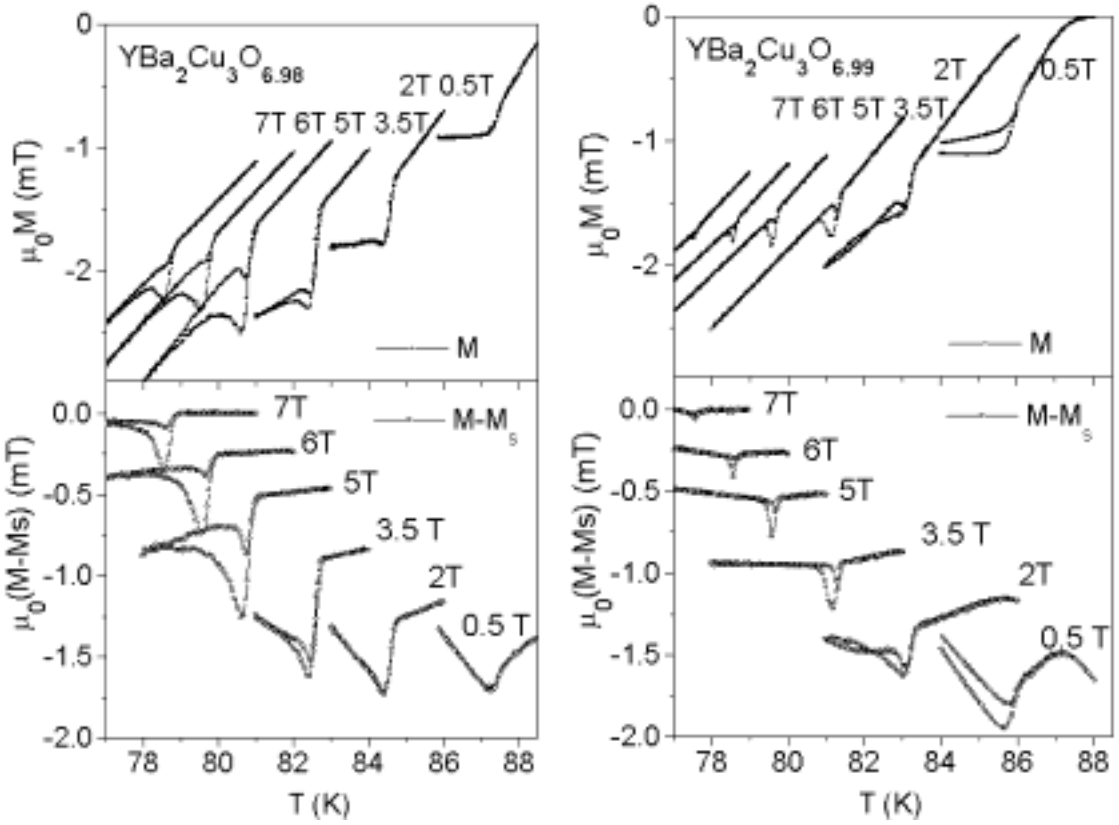

Fig.11. Plots of full (top) and reduced (bottom) magnetizations near the melting transition for sample oxygenations "$O_{6.98}$" (left) and "$O_{6.99}$"(right). The sample was oxygenated at 410^{o}C and 350^{o}C for "$O_{6.98}$" and "$O_{6.99}$", respectively. Note an increase of difference between FCC and FCW magnetizations with increasing magnetic field.

It is shown in Fig.11 that the temperature/field dependence of the inverse λ-peaks is not monotonous. In the sample "$O_{6.98}$", the FCC inverse λ-peaks culminate around 5 T and the FCW inverse λ-peaks culminate around 3.5 T. In the sample "$O_{6.99}$", the FCC inverse λ-peaks culminate around 3.5 T and the FCW inverse λ-peaks culminate around 2 T. Clearly, the magnitude of the inverse λ-peaks decreases at moving along the melting line from these culmination points toward the CP. Concomitantly, the widths of the inverse λ-peaks decrease. It is useful to show at this point how these singularities evolve above the CP. So far, the CP was detected as a point at which the sharp kink in resistivity disappear and the resistive transition start to broaden [11]. López et al [12] have shown that the CP is also a point at which the longitudinal and transverse resistivities (ρ_c and ρ_{ab}, respectively) start to onset incongruently. The dissipation sets in when the correlation between the moving vortices is lost. The in-plane and out-of-plane correlations are lost at different temperatures/fields. It was thus two "melting lines" identified above the CP: one is due to the loss of vortex correlation along the c-axis (along the field) and another is due to the loss of vortex correlation in the ab-plane. Above the CP, the loss of correlation between the vortices in the *ab*-plane is retarded with respect to the outstripping loss of the correlation

along the c-axis. This situation is quite opposite to the one which occurs in the twinned crystals, where by the effect of twinning planes the predominant c-axis correlation between the pancake vortices tends to be preserved longer.

Recently, the CP was observed also using the magnetization measurement [14,25,37]. The CP location was identified in the M vs. H curves at the intersection of the melting line and the fishtail line. Two of the lines at this intersection are well defined. One is the fishtail line well identified with the maximum of J_c. Another one is the low-field branch of H_m, that is the line of 1st order melting transition [14,25,37]. The other lines connected to the CP are ill-defined, as their determination depends on the particular experimental details, e.g. crystal thickness in the V_{top}-V_{bottom} measurements [12].

In this work, the CP is studied for the first time using the measurements of M vs. T curves throughout the transition line. In the highly oxygenated samples, the CP cannot be accessed with the SQUID magnetometer (H_{CP}>7 T). On the other hand, we have found that in the slightly desoxygenated $YBa_2Cu_3O_{7-\delta}$ with $\delta \geq 0.11$ the CP does not occur because the transition is of 2nd order in the overall range of magnetic fields. This situation is shown in the top panel of Fig. 12. Only for the narrow intermediate oxygen contents the CP fall into the range of magnetic fields accessible with our SQUID magnetometer.

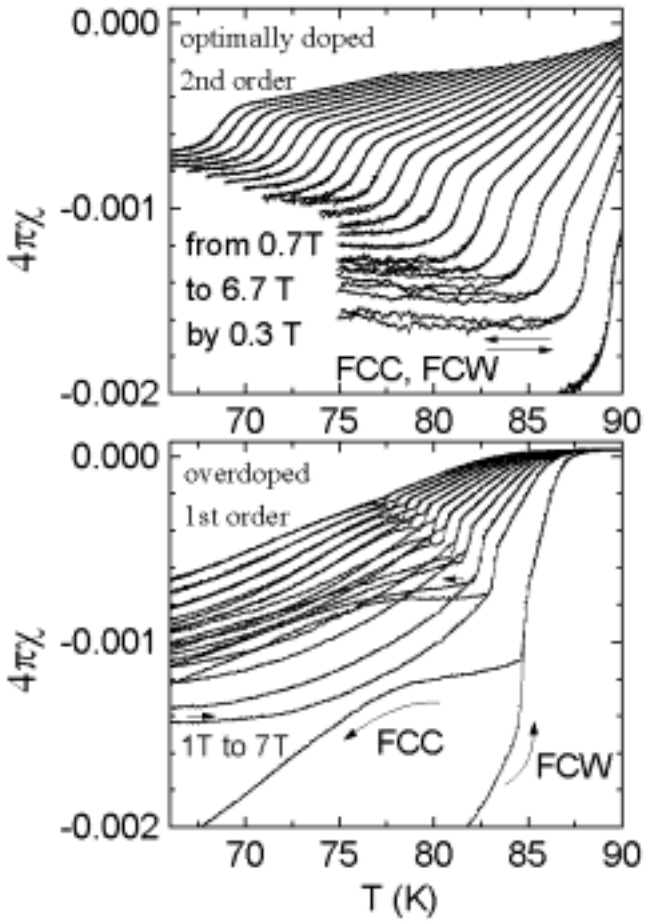

Fig.12. The plots of $4\pi M/H$ vs. T for sample oxygenations "$O_{6.86}$" (optimally doped) and "$O_{6.98}$" (overdoped). Only in the overdoped sample the FCC and FCW magnetization branches are not coinciding.

Figure 12 enables a comparison between the 1st order transition in the sample "$O_{6.98}$" (overdoped) and the 2nd order transition in the sample "$O_{6.86}$" (optimally doped). Here again we go from one sample to another by simply changing the oxygen content in

the same untwinned single crystal. These dense-mesh magnetization data are best demonstrated with using the quantity M/H, shrinking the magnetization scale at large fields. The FCC and FCW branches are divergent only in the sample with higher oxygenation. In the optimally doped sample, the M vs. T magnetization curve is fully reversible on the both sides around the 2nd order transition. Excluding this feature, some similarity between the FCC-behavior of these samples can be recognized for the low-field region. Namely, the FCC magnetization tends to be temperature-independent just below the transition in both samples. On the contrary, in the high-field region the magnetization behaves differently between the two samples. Specifically, in the overdoped sample, the magnetization below the transition follows the slope of reversible magnetization, while in the optimally doped sample it remains temperature-independent. However, the most striking difference between the two samples in this high-field region is in the magnitude of magnetization anomaly. The inverse λ-peak in the overdoped sample appears to be very small compared to the broad σ-like anomaly in the optimally doped sample.

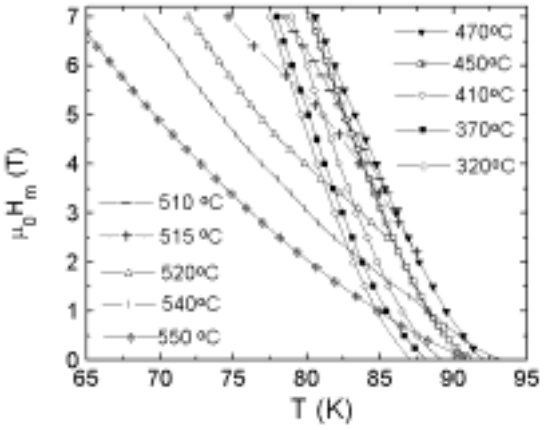

Fig.13. The melting lines in the sample annealed in oxygen flow at different temperatures.

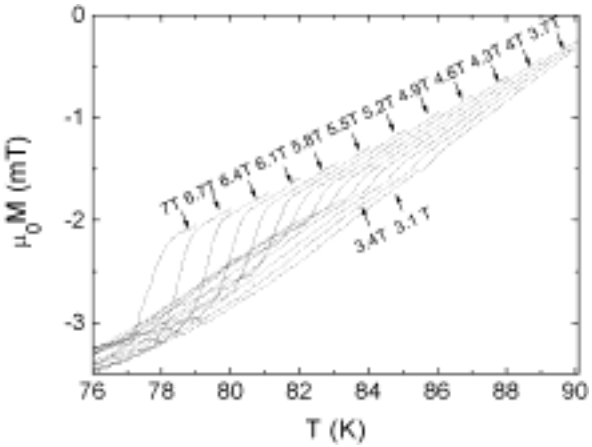

Fig.14. Melting transition near the critical point in the sample annealed at 510°C.

Figure 13 shows the melting lines for a large number of oxygen contents in the same single crystal. It is worth to note that there exist two characteristic slopes for these the melting lines. The larger slope is observed only in highly oxygenated samples, obtained when the crystals were annealed in the oxygen flow below 500°C. The other characteristic slope of the melting lines is at least twice smaller and pertinent to the samples annealed in oxygen at 520-540°*C*. For the intermediate temperatures (510°*C*, 515°*C*, 520°*C*), the melting line consists of two branches. These two branches are connected at the CP.

The jumps in the immediate vicinity of the CP are shown in Fig.14. The huge difference in magnitude between λ-like and σ-like anomalies manifests itself in this Figure as a decrease of the magnitude of the σ-like anomaly as the CP is approached.

The data for the T_c's and for the slopes of melting lines in the samples of Fig. 13 are summarized in Fig.15. The bell-shaped curve of T_c vs. δ is climbed by 1-2 *K* with respect to the flux-grown crystals [38] suggesting the very high purity of our pulling-grown crystals. Moreover, the bell-shaped curve is culminated for the annealing in oxygen at 520°C, which is significantly larger than the optimum annealing temperature for Au-doped crystals[39]. The melting lines were fitted with the 3D XY scaling law

$$H_m(T)=H^*(1-T/T_c)^{2\nu} \qquad (16)$$

where ν=0.669 is the critical exponent for the 3D XY model. In these fits, both H^* and T_c were varied. In spite of very small transition width in our crystals (below 0.3 K), it was observed in the region 7-δ> 6.92, that the fitted T_c's lies within the range of $3\Delta T_c$ to the true value of T_c measured in a small field (10 Oe). The slopes of melting lines H^* observed in the region 7-δ > 6.92 bring together the previously reported values of 139 T[4], 133 T[40], 122.5 T[22], 99.7 T[3], 69.5 T[41].

In the intermediate range of oxygen contents two characteristic slopes coexist for different fields. The steeper slope is associated with the low-field branch of melting transition and the shallower slope is associated with the high field branch of the melting transition. In the fit with Eq.(16) , these two slopes are averaged, and as a result we get in Fig.15 the abrupt change of H^* for these samples (510°C, 515°C, 520°C).

The 2nd order transition near optimal doping shows $\mu_0 H^* \sim 40$ T. This slope is by an order-of-magnitude larger than $\mu_0 H^* \sim 4$T in the $YBa_2Cu_3O_{6.6}$ with T_c of 60K[42].

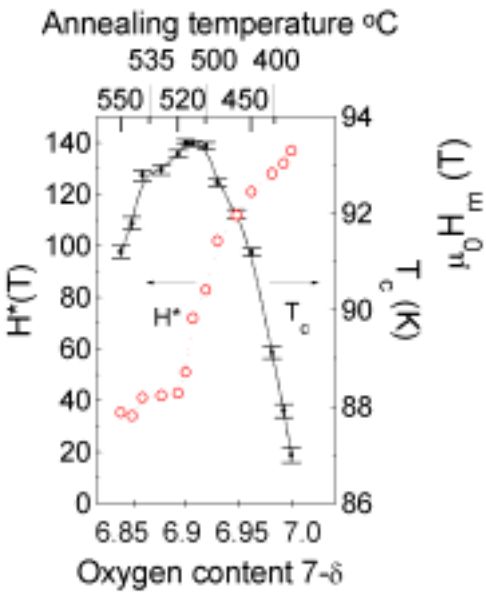

Fig. 15. H^* and T_c vs oxygen content 7-δ. The YBCO single crystal was annealed in the oxygen flow at temperatures shown on the top scale. The oxygen deficiency δ is adapted from the scale of Lindemer et al[9].

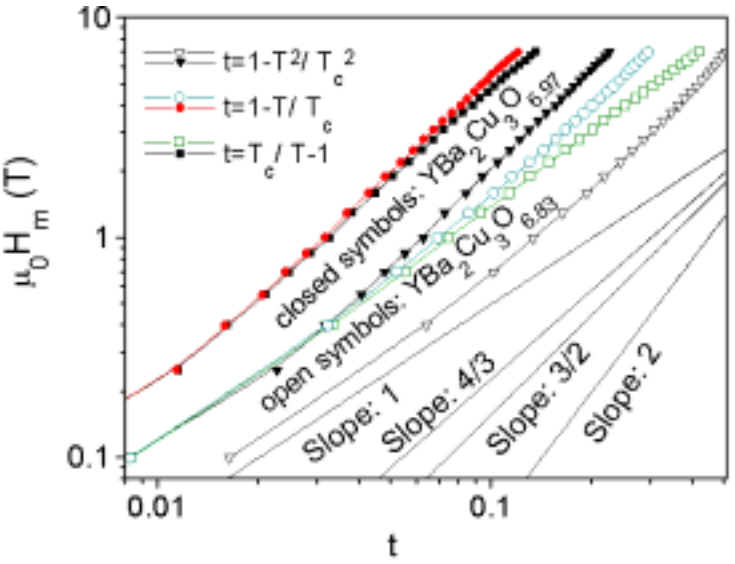

Fig.16. Fields of melting transition in $YBa_2Cu_3O_{6.97}$ (1st order) and in $YBa_2Cu_3O_{6.86}$ (2nd order) plotted against the variables $T_c/T-1$ and $1-T/T_c$. and $1-T^2/T_c^2$. Also shown are the slopes of 1, 4/3, and 2, verifying the theories of decoupling, 3D XY melting, and mean-field, respectively. The slope 4/3 is best for both the 1st order and the 2nd order transition lines.

It is useful to examine whether or not the observed melting lines are consistent with the existing theoretical ideas. For the sake of such a comparison we have plotted the melting fields against the variables $T_c/T-1$ and $1-T/T_c$, which are relevant to the theories of decoupling and melting, respectively (Fig.16). The variable $1-T^2/T_c^2$ is also pertinent to the mean-field approach, as follows from the Eq. (4). The comparison of the slopes in Fig. 16 suggests that the upward curvature of the melting lines agrees best with the 3D XY model [22] for both the 1st order and the 2nd order transitions. It should be noted that except the simplest version of the mean field (Eq.4), the mean-field melting line with H_{c2}-correctinons [43] may fit well the experimental data.VI.

(T,H)-DEPENDENCE OF MAGNETIZATION JUMPS BEYOND THE MEAN-FIELD-BASED PICTURE OF LONDON VORTICES

The London model, in which the phenomenological temperature dependence of penetration depth $\lambda^2(T)=\lambda^2(0)/(1-T^2/T_c^2)$ and the mean field line $B_{c2}(T)=B_{c2}(0)(1-T^2/T_c^2)$ are assumed in accordance with BCS model, describes perfectly the observed shape of the melting line in YBCO with reasonable Lindemann number c_L=0.19 [43]. In order to get this result, Dodgson et al [43] have renormalized the London energy scale $\varepsilon_0 = (\Phi_0/4\pi\lambda_{eff})^2$ and anisotropy ε , introducing a dependence of these quantities on magnetic field. The effective penetration depth thus defined becomes divergent not only near T_c but also near H_{c2}. This correction renormalizes the elastic moduli of line-like flux system in the high-field limit. The shape of the melting line model could be thus adjusted with the numerous parameters to give the experimentally observed temperature dependence with clearly lower curvature than that given by Eq.(4).

Retaining unaltered the mean-field line, $H_{c2}(T)=H_{c2}(0)(1-T^2/T_c^2)$ is an additional assumption made in the field-induced renormalization of the London energy scale [43]. In YBCO, however, the line H_{c2} is totally cleared away by thermal fluctuations. There is no indication that the mean-field picture should be retained. The 3D XY model [22] suggest that the line H_{c2} can be described by the power law $(1-T/T_c)^{1.338}$. In this case, the melting line H_m represent the line H_{c2}, suppressed by thermal fluctuation, $H_m=CH_{c2}$, with the temperature-independent factor $C=const$. The hyperscaling [44] suggest also that C should not depend on the oxygen content, except the case when the order of transition changes with changing the oxygen content [14]. It is plausible to reverse the melting line fitting and use the analytical expression for the melting line, Eq. (16), to obtain the (T,H)-dependence of the magnetization and entropy jumps. With this prescript, the temperature dependence of magnetization jumps is given by Eq.(13) in which $\lambda(T)$ is substituted by $\lambda_{eff}(T)$. Then the entropy per vortex per bilayer ΔS_d and its configurational part ΔS_{0d} are found from ΔM according to the Clapeyron-Clausius equation:

$$\Delta S_d = -\mu_0 \Delta M d\Phi_0 (dH_m/dT_m) B_m^{-1}$$

$$\Delta S_{0d} = \frac{\mu_0 \Delta M d\Phi_0 (dH_m / dT_m)}{\left(1+\frac{2T}{\lambda}\frac{d\lambda}{dT}\right) B_m} \qquad (17)$$

Because the Eq.16 fits well the experimental data, we substitute into the Eqs.(13) and (17) the temperature dependence of penetration depth in the 3D XY model:

$$\lambda_{eff}(T) = \lambda(0)_{eff}(1-T/T_c)^{-\nu/2} \qquad (18)$$

This function for penetration depth for $\nu \approx 2/3$ was also found in the zero-field microwave experiment [45]. Curiously, the argument $T_c/T-1$ relevant of the decoupling (sublimation) hypothesis [46] appears to give the enhancement factor of entropy in Eq. (17):

$$2T\lambda^{-1} d\lambda/dT = \nu(T_c/T-1)^{-1} \qquad (19)$$

Compared to the mean-field λ (ν=1), the divergence of λ_{eff} near T_c is slower. If we directly apply the final result for ΔM using the Eq. (15), then the ΔM falloff near T_c is slowed down:

$$\Delta M \sim (1 - T/T_c)^{\nu} \qquad (20)$$

This expression is in improved conformity with the weakness of the temperature dependence of the magnetization jumps observed in our experiment. On the other hand, the non-monotonous behavior of ΔM vs. T is still not described by the Eq. (19). This disagreement could be related with the corrections to be introduced in the volume per elementary degree of freedom. The temperature dependence of the entropy jumps given by Eqs. (9) and (10) is different than that given Eqs. (17) with ΔM substituted from Eq. (20). The estimation of the number of elementary degrees of freedom given by $1/\varepsilon a_0^3$ ignores the disorder in a sample. Since by changing the oxygen deficiency in a sample we can move the location of the CP, N_{edf} is scaled not only with field and anisotropy but also with disorder. The disorder thus leads to the nonmonotonical dependence of ΔM vs T.

VII. FIELDS PERPENDICULAR TO C-AXIS

The inverse λ-peaks in the M vs T curves were observed also in a geometry of tilted fields and for $H \perp c$. The magnetization jumps at closing the M-H loops were also observed for fields parallel to Cu-O chains ($H // b$). Figure 17(a) shows the inverse λ-peak observed at field-cooling (FCC) for $H // b$ and warming (FCW, ZFCW) modes.

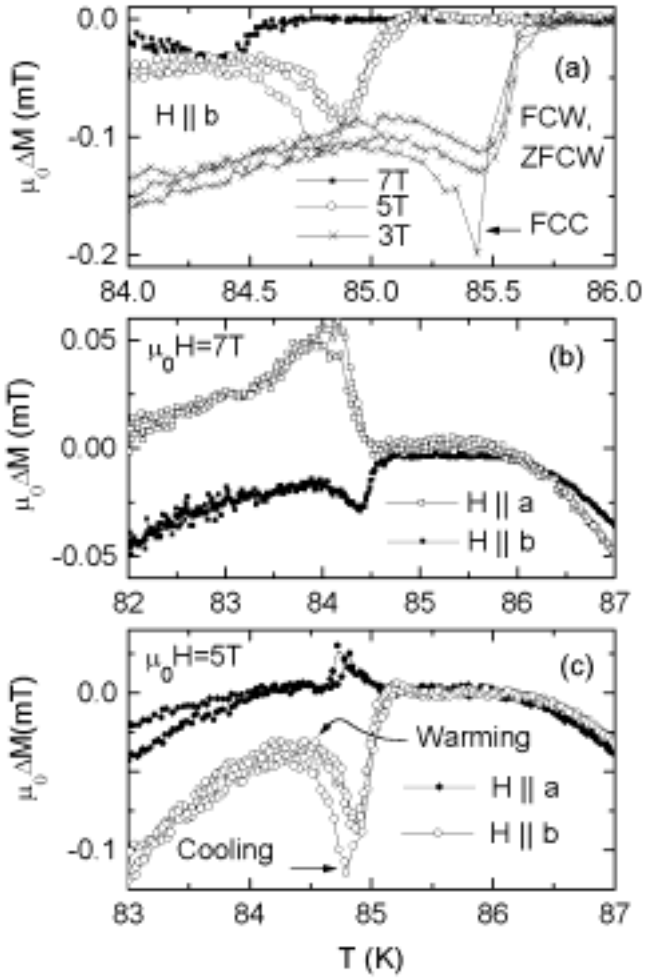

Fig. 17. (a) Magnetization jumps for warming the untwinned sample cooled in field (FCW), in zero-field (ZFCW) and for field-cool cooling (FCC) for fields of 3T, 5T and 7T applied along the b-axis; (b) for field of 7T along a and b axes; (c) for field of 5T along a and b axes.

The inverse λ-peak observed at field-cooling (FCC) for $H//b$ is larger than that observed at warming (FCW, ZFCW). Surprisingly, the λ-peak reverse its sign in the orientation ($H//a$), in other words, for the fields in the ab-plane perpendicular to Cu-O chains. The field dependence of the amplitude of the λ-peaks is also reversed for this orientation of the field. It is shown in Fig. 17 (b), (c) that the magnitude of the λ-peak decreases with decreasing field. This is in contrast to the field dependence of magnetization jumps in both ($H//b$) and ($H//c$) orientations. Figure 18 shows the magnetization jumps at closing the hysteresis loops M vs H. These jumps shows smaller magnitude than the jumps for the same temperatures in Fig. 9. Even compared in the same range of magnetic fields (3-6T) the jumps are smaller in the ($H//c$) orientation than in the ($H//b$) orientation, if the same value of the measurement step ΔH is employed. However, compared to the level of reversible magnetization, the jumps are larger for ($H//b$) than for ($H//c$).

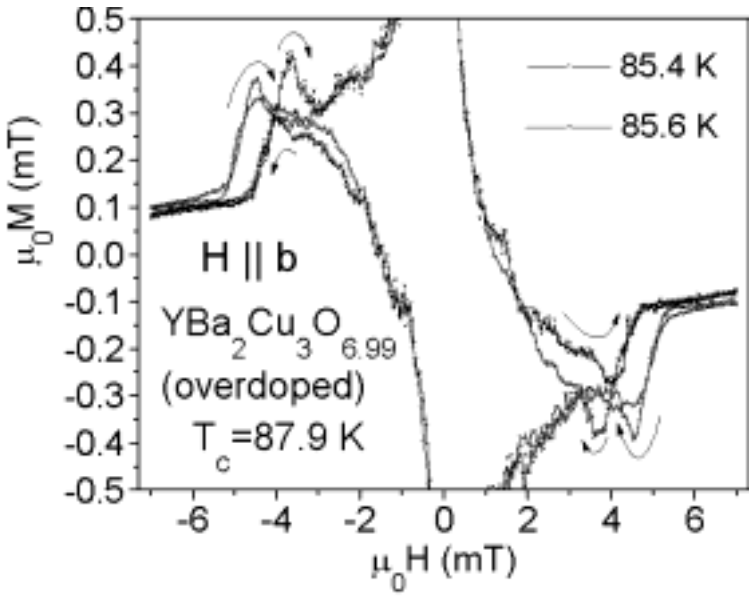

Fig.18. *M-H* hysteresis loops obtained for ($H//b$) in $YBa_2Cu_3O_{6.99}$ at 85.4K and 85.6 K. The sample was annealed at 350°C.

The observation of the angular-dependent magnetization jumps (λ-peaks) is in agreement with the fact that the magnitude of these anomalies is much larger than that expected from the typical latent heat. The latent heat of vortex-lattice melting for varying angles Θ between the magnetic field and c-axis was recently measured [47]. It was found that the latent heat depends solely on the temperature and does not depend on Θ or melting field. This is not in disagreement with our data because the λ-peaks are associated with premelting peaks and the fast relaxation of these singularities takes place. The scenario, in which a few residual twinning stripes are fully responsible for the premelting peak [30], is not plausible because the premelting peak does not vanish for ($H//b$) or for ($H//a$). The reason for deviation of the magnetization anomalies from the expected fully 3D behavior could be related to vortex tilting instabilities at large angles (Θ~90°). It was observed recently in $YBa_2Cu_4O_8$ that the resistive transition shows anomalous behavior at large angles above the "melting" kink [48]. These anomalies were interpreted to be produced by a competition between the intrinsic pinning and the intervortex interactions. We believe that the intrinsic pinning should indeed suppress the admixture of the 2nd order character phenomena observed at the melting transition in our samples.

VIII. THE EFFECTS OF COOLING RATE, "NON-DIPOLAR" SQUID RESPONSE AND SAMPLE QUALITY

The melting transition manifests itself in the magnetization in the form of jumps ΔM or inverted λ-peaks depending on the relative influence of several effects. The most important of them are the rate of temperature/field sweep/stepping, the "nondipolar" response of the SQUID magnetometer and the sample quality. In the SQUID magnetometer, the sample is scanned through a set of pick-up coils arranged into a second derivative gradiometer configuration [49]. We collected the data using various scanning lengths starting from 0.2 cm. The MPMS software accepts settings for scan length in the range from 0.1 cm to 12 cm. Operations with small scanning lengths are not conventional because the data collected in this regime are more sensitive to the non-ideal shape of the SQUID gradiometer output signal $V(z)$. The procedure of sample centering may require many iterations for small scanning lengths. This difficulty is avoided by following a sequence of operations: (i) centering the sample with larger scan length; (ii) setting smaller scan length; (iii) adjustment sample position; (iv) recentering sample with small scan length. The step (iv) may not require then centering reiterations for perfect centering of the sample for even very small scans.

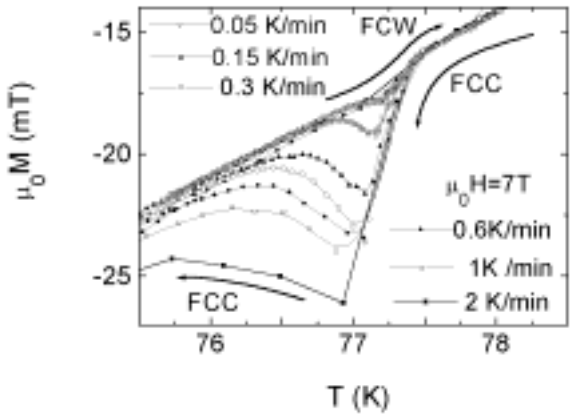

Fig.19. FCC and FCW magnetizations in the field of 7T measured with different rates of cooling and warming.

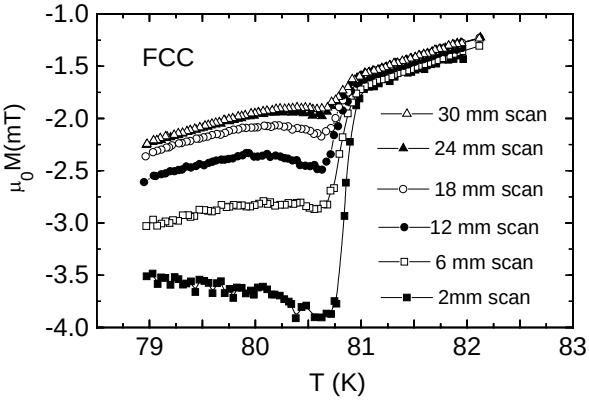

Fig.20. Dependence of the FCC magnetization on the scan length. The sample is overdoped at 410°C (T_c=89.1 K)

The dependence of the magnetization on the cooling rate is the most clear evidence that origin of the inverse λ-peaks is non-trivial. Figure 19 shows the FCC and FCW magnetizations near the first order transition measured with different rates of temperature sweep. The data were obtained with the scanning length of 16 mm. Figure 20 shows the sample magnetization data obtained in FCC mode with a rate of 0.18 K/min and with different scan lengths. The sample for this measurement was annealed at 410°C and it shows the melting transition at 81K in the field of 5 Tesla. Clearly, the scatter of data obtained with different scanning lengths is only a few percent above T_m, however the data differ twice or so below T_m. These data show that an additional factor appears below T_m which makes the measured magnetization value dependent on the scan lengths, at least when the latter was set to be small enough. The dependencies observed for different values

of the applied field are very similar. The data obtained for two different fields at warming (FCW) and cooling (FCC) of the fully oxygenated sample are shown in Fig.21. These data are as well scan-length dependent below T_m. It is well known that a vortex glass displaying a hysteresis at a 1st order transition may show a very broad distribution of relaxation times [50]. Both the time at which sample was exposed below T_m and the cooling rate should affect the hysteretic behavior near the transition [50,51]. Despite the cooling rate was fixed in the measurements shown at Figs.20,21 as well as the warming rate itself was constant (0.18 K/min) one observes clearly the effect of scanning length.

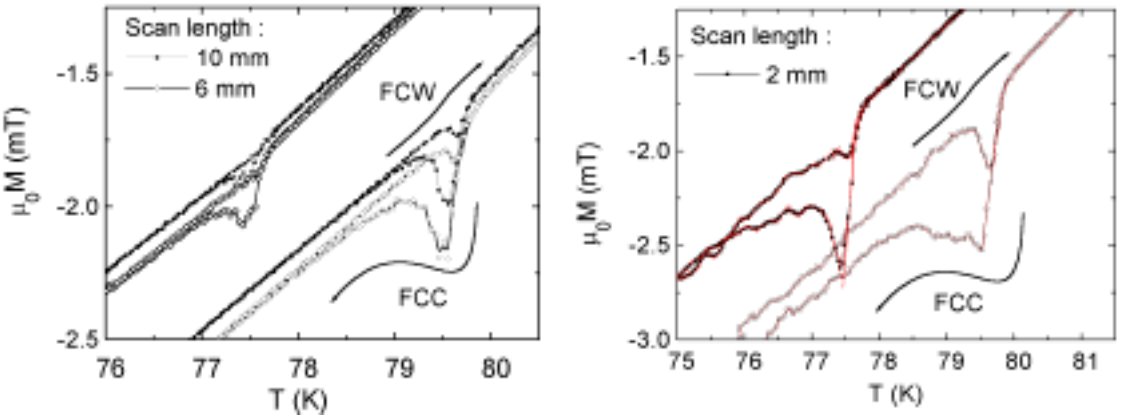

Fig. 21. The inverse λ-peaks of the magnetization for fields of 5T and 7T in the fully oxygenated sample. The FCC and FCW magnetizations were measured with the scan length of 10 mm, 6mm (left panel) and 2 mm (right panel).

The difference between FCC and FCW data becomes more pronounced when the small scan lengths are used. Because such a difference could be clearly observed for small scanning length, it can be argued that previously claimed reversible character of magnetization below T_m [4] is not likely even for "good" samples. It was argued previously [4], that the reversible behavior of the field-cooled magnetization could be observed well below the melting transition in "good" crystals, and such a feature would certify the high quality of the samples. However, the magnetic response can be clearly distinguished between the vortex phase regions above and below the melting line $T_m(H)$, and the irreversible behavior could be reconstructed as soon as $T<T_m$ using the available regimes of operating the SQUID gradiometer. This is quite an original result since for the conventional mode of SQUID-measurements the "reversible" behavior of $M_{FC}(T)$ magnetization was also observed in this work, which suggest, in fact, similar quality of the crystals. We argued [13] that these discrepancies originate from the appearance (just at the melting transition) of the "non-dipolar" contributions into magnetic response of the samples.

Above T_m the SQUID output signal can be well approximated by the response function of a point magnetic dipole with coordinate ζ at the axis of a second derivative coil gradiometer [49]:

$$h(\zeta) = -1/2R^2((R^2+(\zeta-L)^2)^{-3/2} + (R^2+(\zeta-l)^2)^{-3/2} + (R^2+(\zeta+l)^2)^{-3/2} + (R^2+(\zeta+L)^2)^{-3/2}) \qquad (21)$$

where R is the radius and L and l are the vertical positions for the two sets of the second derivative gradiometer coils. The shape of a distorted SQUID output signal below T_m can

be understood from the principle of reciprocity between the magnetic flux Φ produced in a gradiometer coil by a magnetic moment $\boldsymbol{\mu}$ and a magnetic field $\boldsymbol{B}$ produced by the same coil carrying a current I [52]:

$$\Phi I = \boldsymbol{mB} \tag{22}$$

By allowing some variation in magnetic response of the sample as it is scanned along z and letting the specimen to have a finite size the following expression for the SQUID voltage in function of position z can be derived from Eqs.(21,22) [51]:

$$V(\zeta)=m(z)h(z)+q(z)h_{\zeta}'(z)+o(z)h_{\zeta\zeta}''(z)+...) \tag{23}$$

In this expansion series, m, q and o stand for the dipole, quadrupole and octupole moments which can be calculated by integrating over a specimen of a finite size the expressions $m(\boldsymbol{r})$, $zm(\boldsymbol{r})$, $(3z^2-r^2)m(\boldsymbol{r})/2$, respectively [53]. In the latter expression (Eq.23), all the moments m, q and o are allowed to depend on the position of the sample in the solenoidal magnet. Such a dependence may be produced if the sample is pulled through non-uniform magnetic field during the measurement scan. The purely dipolar SQUID output signal correspond to the following conditions:

$$\begin{gathered} m(z) = const \\ q(z) = 0 \\ o(z)=0 \\ ... \end{gathered} \tag{24}$$

The estimates of what condition among those listed in Eqs.(24) is broken to cause the observed "non-dipolar" SQUID signal should be taken with caution since the inbuilt MPMS software displays the voltage $V(z)$ resulted after subtraction of the linear drift. Therefore, the odd-order-derivative poles (quadrupole, 16-pole, 64-pole) are interfered in the fitting procedure with the linear "drift" terms, so that the resulting odd moments could not be ascertained until the fit is done in the much larger scan range than the employed scan (e.g. from -2 cm to 2 cm). The larger scan, however, will involve the measurement in less homogeneous field, which could destroy the inhomogeneous FC state.

Whether or not retaining more than one term in the Eq.(23) is essential for explaining the "non-dipolar" SQUID output signal was a confusing point in a number of previous works [13, 53-58]. The plausible variation of the dipolar response $m(z)$ with z was searched in this work to explain the observed "non-dipolar" effects in $V(z)$. The problem was to find the flux flow effects which may produce a quick variation of $m(z)$ near the center of the scan, so that decreasing the scan length leads to a rapid increase of the absolute value of the measured output signal.

It is worth to note that besides the tiny field inhomogeneity which may lead to the condition $m(z) \neq const$, and the finite sample size which gives $q(z) \neq 0$ and $o(z) \neq 0$, there could exist another factor changing the shape of SQUID output signal, which is difficult to reproduce and control. In the fully oxygenated sample, we have performed the additional experiments to reproduce the narrow inverse λ-peaks shown in Figs.3 and 21. The time of a few weeks was elapsed between the first and the second experiments. Figure 22 shows the data obtained in the second experiment. The measurement conditions in the second experimental setup including scan length and the sample attachment were reproduced as closely as possible. However, the λ-peaks observed in the second experiment, are significantly broadened (Fig. 23).

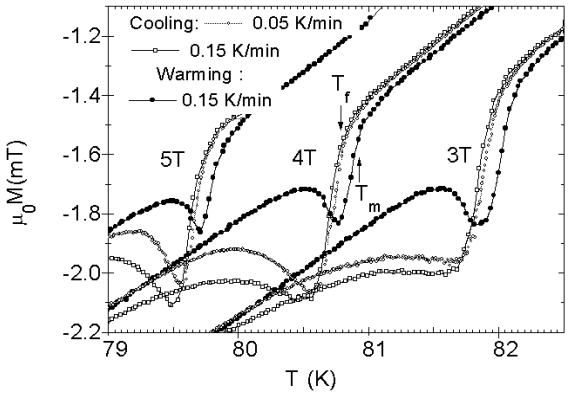

Fig.22. The FCC magnetization measured in fields of 3, 4 and 5 Tesla with cooling rates of 0.05 K/min and 0.15 K/min and FCW magnetization measured at 0.15 K/min in a fully oxygenated YBCO single crystal. The sample and the scan length (1.6 cm) are the same as in Fig. 3. The temperatures T_m and T_f are affected neither by an experimental setup, nor by a time elapsed from the sample preparation, however, the behavior of magnetization below T_m (T_f) is changed.

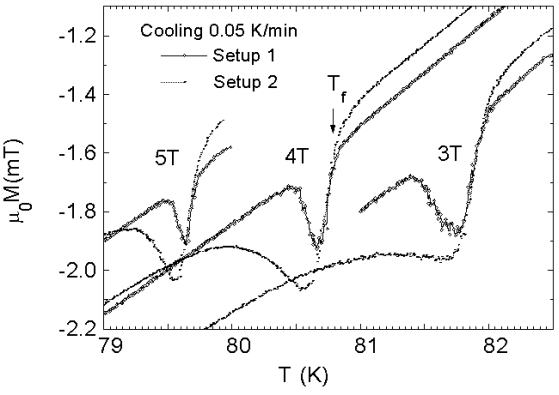

Fig.23. Comparison of the FCC magnetization measured in fields of 3,4 and 5 Tesla with the cooling rate of 0.05 K/min between the two experimental setup shown separately in Fig.3 and in Fig.22. Note the exact coincidence of the right-hand shoulder of the inverse λ–peaks.

Various explanations of the distorted $V(x)$ were discussed previously [13,59]. Except for the intrinsically inhomogeneous FC magnetic state, the inhomogeneity of the applied magnetic field and the formation of the transverse field component in the sample were analyzed as the possible external sources of the observed inhomogeneous magnetic state[59]. Concerning the transverse magnetization component as another possible source of the distorted SQUID signal suggested previously for the thin films[59], it is clear by now that the transverse dipole passing through a second derivative coil array should result in zero response function due to symmetry. Recent calculations [60] showed that if such a dipole is off-centered from the axis of the gradiometer, then it could, indeed, induce the distortion of $V(z)$. However, corresponding component of the voltage is asymmetric with respect to the center and could be mixed in the fit with the "quadrupolar" response term. The latter could not be ascertained from the typical measurement because the odd terms in the expansion series (Eq.4) should mix for short scanning lengths with the subtraction of linear "drift" term employed in the MPMS software.

The possibility variation of $m(z)$ with z-coordinate was discussed extensively with regard of the distorted SQUID signal observed in the YBCO thin films[59,61-63]. Libbrecht et al [61] discussed the situation when the measured dipolar moment would acquire a z-dependence due to the non-uniformity of the magnetic field along the axis of the solenoidal magnet. When the sample is pulled through the non-uniform field, the removal and backloading of vortices occurs in conformity with the pinning properties of the sample. Below the irreversibility line the field variation during the cyclic sample motion would produce the minor hysteresis loops (MHL). Wrapping the MHL at each measurement cycle results in a change of sample magnetization $m(z)$ during the cycle and could produce the distorted SQUID signal $V(z) = m(z)h(z)$ [61]. The calculations of MHL[61] were in a good agreement with the experimental data for YBCO thin films[59,61,62] in a case when the external field was assumed to have a minimum in the

center of gradiometer coils array. The minimum in the field profile was observed in the center of the magnet at small applied fields [49,64]. In such a case, the reduction of the field in the center of gradiometer was argued to produce a reduction of the absolute value of magnetization. The latter was implied to reverse sign near T_c due to such an effect, which was observed close to T_c, while far below T_c the distortion of the SQUID signal was observed to vanish [49,59,61,62]. The undistorted low-temperature shape of the signal $V(z)$ was explained by relatively small variation of the magnetization at wrapping the MHL due to the increased critical current at lowering temperature[61]. A characteristic profile $V(z)$ in Refs.[49,59,61,62] exhibits a reversal bump near the center of gravity, which is clearly different from $V(z)$ observed in our work [13].

The employed scan length start to affect the measured value of the magnetization below T_m as a result of divergence between measured curve $V(z)$ and inbuilt MPMS fit function $h(z)$. The observed central peak of $V(z)$ is sharper than that for $h(z)$. With smaller scan length the fit function mimics the enhanced curvature of $V(z)$ by increasing the value of m_0, which is the factor of the derivative $dV/dz=m_0dh/dz$. The sensitivity of data to the shape of $V(x)$ is enhanced when the scanning lengths is reduced. This leads to the typical scan-length-dependence of the measured magnetization as shown in Fig.24.

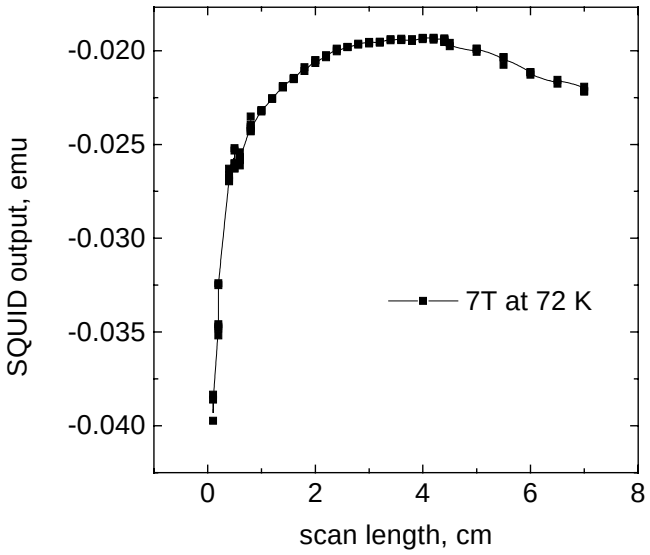

Fig. 24. Scan length dependence of the magnetic moment in a field of 7T at 72 K. The value of H_m in the field of 7T in this sample is 79.5 K.

We attempted to rule out the explanation of the distorted SQUID signal due to MHL in our previous work [13]. First of all, the effect of field inhomogeneity should vanish at very small scanning lengths, however the effect showed an apparent increase. Furthermore, our approach [13] was based on the observation of the effects of field inhomegeneity at very large scan lengths and at low temperatures where J_c is large. When the scanning length exceeds the value of 54 mm the measured $\mu_0 M$ starts to grow progressively with increasing scanning lengths. The field reduction occurs at the edges of the scan (>54 mm), where the signal from the second derivative coil array is very small. In this case, the MHL leads to the development of the "homogeneous" Bean critical state which result in the ideal shape of $V(z)$ signal in the center of the scan (-25mm<z<25mm). For large J_c's the field inhomogeneity manifests itself clearly when the scan length exceeds 54 mm. We concluded that the field inhomogeneity in the center of scan is very small. On the contrary, Roy et al [65] have explained the curious effects of scan lengths by the enhanced field

inhomogeneity in the center of the SQUID magnet. In this work, we propose a model, which could explain approximately the observed dependence of the SQUID output signal on the scan length by taking into account the observed rapid relaxation. In this model, the magnitude of field inhomogeneity is not essential, however, the sign of dH/dz is important. Due to symmetry dH/dz changes sign in the center of magnet. Figure 25 shows

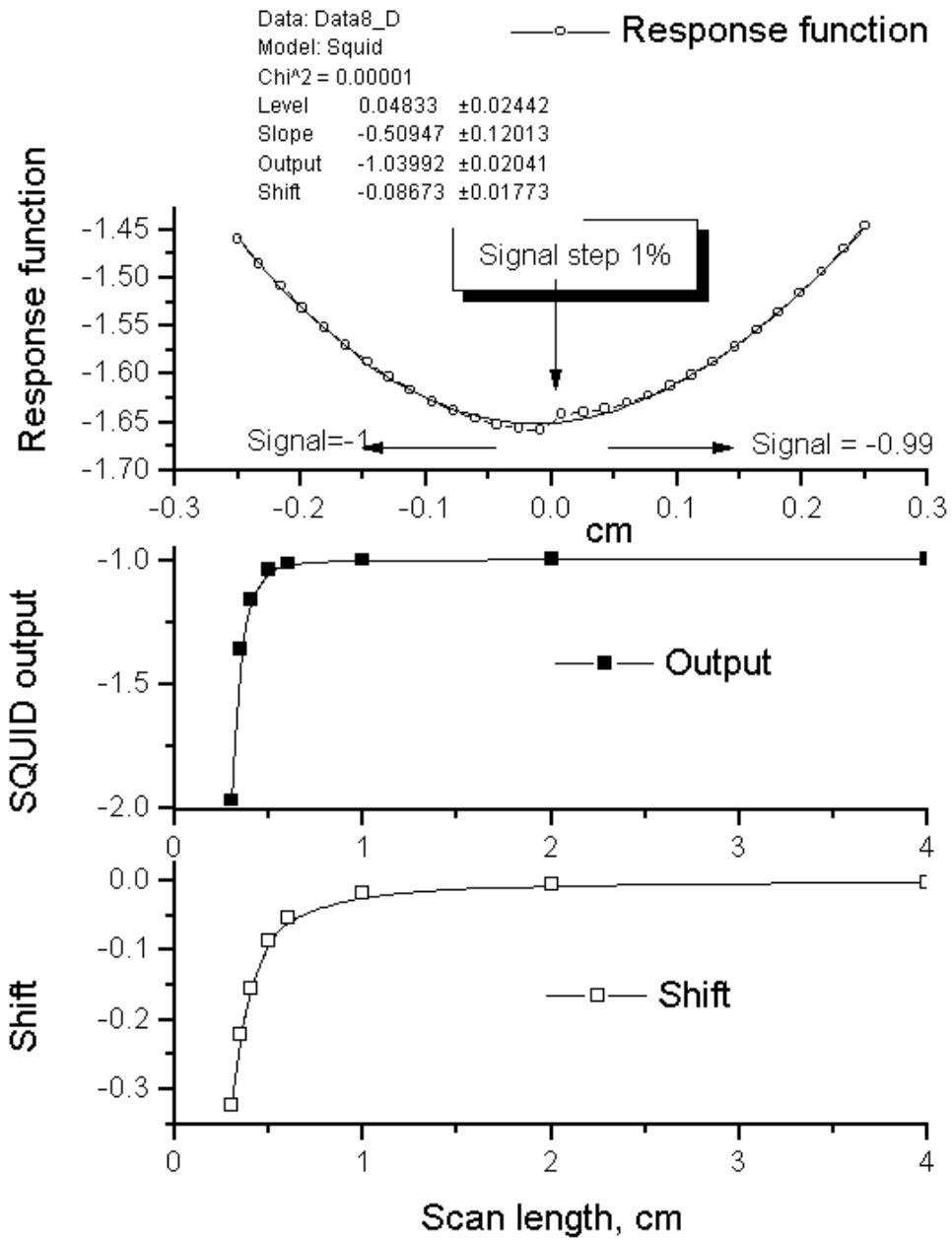

Fig. 25. Top: Product $h(z)m(z)$ for $m(z)= -1+0.01sgnm(z)$(circles) and the fitted function $m_{MPMS}h(z-z_0)$ (line) for the scan lengths of 0.5 cm. Middle: the scan lengths dependence of the "MPMS SQUID output" m_{MPMS} determined from fitting the function $m_{MPMS}h(z-z_0)$ for the product $h(z)m(z)$. Bottom of figure: The scan length dependence of the fitted off-centering z_0.

the result of fitting of the product $h(z)m(z)$ with the function $m_{MPMS}h(z-z_0)$. We assumed that $m(z)$ changes with z in a step-like manner. The step $\Delta m=0.01m$ occurs in the center of the scan, $z=0$. This step arises from the finite reaction of the flux flow in the solid phase on the sign of the field gradient. Such a step-like anomaly appears even when

$J_c=0$. When the scan lengths is reduced, the output signal m_{MPMS} delivered by the MPMS software start to deviate from m=-1. The absolute value of m_{MPMS} increases with decreasing the scan lengths in accordance with the experimental data (Fig.24). In the experiment, the scan-lengths dependencies similar to those shown in Fig.24 can be obtained even when z_0 is fixed in the fitting algorithm. Although this model cannot clearly explain the latter result, this model gives the idea on the origin of the singularity in the center of the scan.

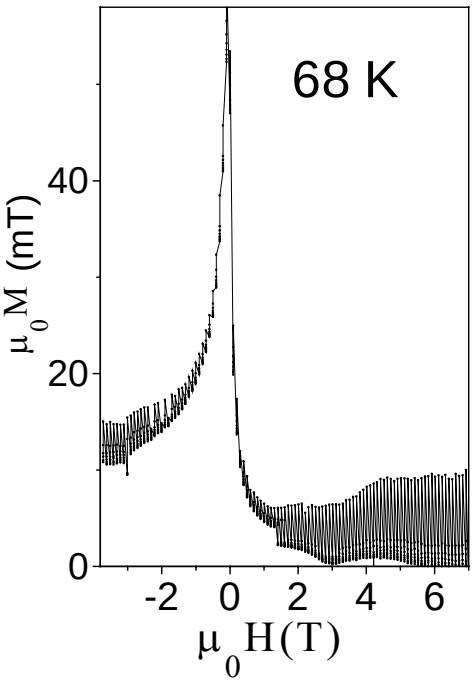

Fig.26. Magnetization $\mu_0 M$ vs. applied field $\mu_0 H$ measured in a slightly less clean overdoped sample at 68 K. The data were collected at the reverse branch of the hysteresis loop. The measurement was done at each value of the applied field eight times during 100s.

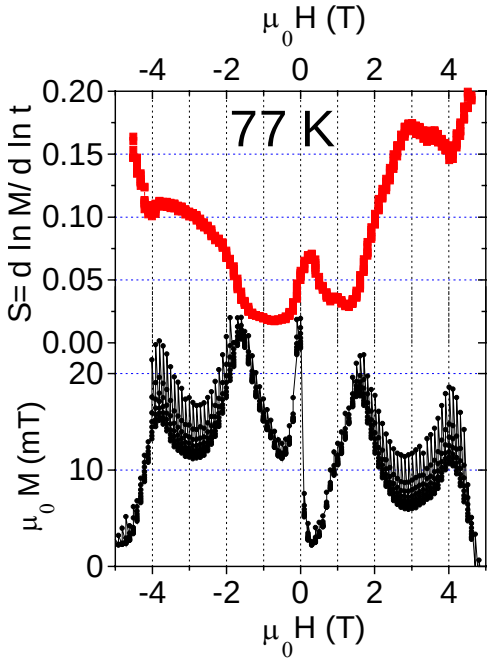

Fig.27. Same sample as in Fig.26, however, at 77 K. The data were collected at the reverse branch of the hysteresis loop. The normalized creep rate $S=d\ln\Delta M/d\ln t$ is calculated from averaging the derivative data for last six measurement of the total eight.

Finally, let us discuss briefly the effect of impurities on the melting transition. Figures 26 and 27 show the flux pinning and creep phenomena in the slightly impure crystals grown by the same technique [66]. In the overdoped state, these crystals show the similar T_c of 87 as pure crystals, however, by optimal doping the T_c value can be raised only up to 92.5 K instead of 93.5 K. Although at low temperature (Fig.26) the hysteresis loops are qualitatively similar to those shown in Fig.10 (d), the fishtail effect does not disappear at higher temperature (Fig.27). Instead of the premelting peak one sees in Fig.27 the split fishtails. Different explanations are proposed for the fishtail splitting [14,66]. The rate of the flux creep changes with field following the oscillations of the logarithmic derivative of J_c. At approaching the irreversibility line the critical current decreases gradually from the very large peak values. Correspondingly, the flux creep rate increases slowly at approaching the transition and no clear melting transition can be seen.

IX. DISCUSSION

Our analysis [67] suggests that there exist the intrinsic origin of the observed non-monotonic behavior of magnetization jumps unrelated to the experimental artifacts. Along the 1st order transition line, the magnitude of the jump ΔM culminates at a point located below the CP. The mean-field-like monotonous decrease of ΔM at approaching T_c may correspond, in principle, the right-hand shoulder of the overall curve ΔM vs. T. Several origins for the existence of the extremums in ΔM along the melting line are known up to date. The vortex loop theory [68] suggest that the equilibrium vortex density is perturbed after quenching through the transition. In its standard form, this theory is applicable rather close to T_c. In analysing the experimental data, we bear in mind that the character of transition may change even several times when going along the melting line.

First of all, the diamagnetic fluctuations render a substantial difference between the relevant fields H, B and H_{app} at very small fields. This leads to the inverse 3D XY scaling for $H<10^{-5}$ Oe and $T-T_c<10^{-7}$ K [69]. Approaching the transition the 3D XY correlation length diverges more rapidly than the penetration depth (Eq.18):

$$\xi_{ab}(T) = \xi_{ab}(0)(1-T/T_c)^{-\nu} \tag{25}$$

The point of 3D XY inversion is determined from the equation

$$\xi_{ab}(0)(1-T/T_c)^{-\nu} = \lambda_{eff}(0)(1-T/T_c)^{-\nu/2} \tag{26}$$

Because the condensation energy in the 3D XY model is proportional to $\xi(0)^{-2}$, a rapid increase of $\xi_{ab}(0)$ is evident from the relationship

$$\xi_{ab}(0) \sim (H^*)^{-1/2} \tag{27}$$

where H^* is the melting field extrapolated to zero temperature (Fig. 15).

Second factor which causes a change of the nature of melting transition at moving along the melting line is the effect of low-field pinning associated with zero-field peak of critical current. It is assumed in Eq.2 that the width of the zero-field peak scales with temperature very similarly to the scaling of melting line:

$$H_0 = H_0^*(1-T/T_c)^{2\nu} \tag{28}$$

In the case when both scalings, Eq. (16) and Eq.(28) are fulfilled simultaneously, no change of pinning effect along the melting line is expected. However, if one of these scalings breaks down (e.g., in the optimally doped samples), the pinning associated with the zero-field peak become non-equivalent for different melting fields. We have observed in Sec. II that most frequently the pinning effect on melting transition is more efficient at low fields than at high fields. Also, this effect is probably at the origin of a general trend to smoother low-field transition observed in neutron diffraction intensities [70]. The intensity of a diffraction reflection integrated over its full rocking curve is proportional to λ^{-4}. With the Eq.(18) taken into account this leads to $I(t)=I_0(1-t)^{2\nu}$ [70]. The plot of the experimental values of 2ν vs. H_{app} in Ref. [70] shows that 2ν is slightly larger than 4/3 for small fields, but smaller than 4/3 for higher fields. Our results show a similar deviations in the shape of the melting line. The $H_m(T)$ curve is best described by the exponent $2\nu=4/3$ only in average. By varying the fitting range , we have found that 2ν is larger than 4/3 if the fit is done in a range limited by 2-3 Tesla in overdoped sample. In the same range, we

have observed the effect of pinning on the shape of magnetization discontinuity. Nevertheless, the 3D XY scaling (Eq. 16) fits the melting curves much better than either the sublimation law, $T_m \sim (T_c/T-1)$, or the mean–field law without H_{c2} corrections, $T_m \sim (1-T^2/T_c^2)^2$.

It was also observed by calorimetry that several different regimes of melting depending on magnetic field exist separated by lower and upper critical points [71-73]. The melting regimes separated by the upper CP are the melting of lattice-like Bragg glass and melting of dislocation-rich vortex glass. In accordance with our results, Langan et al [74] have observed a strong increase of H_{CP} with decreasing oxygen deficiency. It is worthy of note the analogy and the difference between the phase diagram of polydispersed hard sphere mixtures [75,76] and the vortex phase diagram. The oxygen deficiency δ in $YBa_2Cu_3O_{7-\delta}$ plays a similar role as a polydispersity σ, defined as the ratio of the standard deviation to the mean diameter of the distribution of hard spheres. When δ or σ increases the absolute value of density discontinuity at the transition $\Delta\rho=\rho_s-\rho_l$ decreases. The difference of densities $\Delta\rho$ is positive for the Bernal spheres and negative for the vortex phases. The discontinuity $\Delta\rho$ vanishes at the terminal polydispersity point $\sigma_t \sim 0.08$ [77] and at the CP for $\delta_{CP} \sim 0.11$ (at $H_{app}=0$)[14]. In fact, the critical oxygen deficiency is a function of field, so that $\delta_{CP}=0.11$ is true only for zero field. We have observed [14] that δ_{CP} varies slowly with field, so that for $\mu_0 H=7$T the critical oxygen deficiency is $\delta_{CP}=0.06$. In other words, H_{CP} strongly increases with decreasing δ, as is also stated in other works [37,74]. Taking into account the analogy with the polydispersed hard spheres, the origin of the decrease in magnetization jumps ΔM at approaching to the CP along the melting line becomes clear. We observed indeed in the present work that the curve $\Delta M(H)$ culminates at the intermediate fields. In accordance, the location of the maximums on these curves is dependent on the oxygen deficiency. These disorder-induced phenomena are not apprehended yet in the most of the recently developped theoretical considerations [8,43].

In the system of the polydisperse Bernal spheres, there exist a range of polydispersities in which the crystallization transition is reentrant [77]. If our analogy is thoroughgoing, we must conclude that the low-temperature vortex state is somewhat more disordered than the vortex crystalline state just below the transition. The observed admixture of the 2nd order transition could be related to this reentrant crystallization.

The nature of the lower CP observed in Refs.[71,73] is less clear. The melting of a vortex crystal into a disentangled liquid breaks both gauge and translational symmetries. This breakdown is to occur simultaneously only at the 1st order transition line between the lower CP and the upper CP. In the low-field limit the melting could be reentrant and proceed in two stages [9]. While the upper CP is clearly related to the pointlike disorder, the origin of lower CP could be in the divergence of the melting and decoupling lines below the lower CP.

One more factor which may produce a change of nature of melting transition at moving along the melting line is the reorientation of the vortex lattice. This factor originates from the occurrence of chains in the structure of $YBa_2Cu_3O_7$. It was observed by the small-angle neutron scattering that the hexagonal vortex lattice is aligned by its corner with the a axis at small fields (0.2 T), but with the b-axis at larger fields (above 3T)[78]. Unfortunately, this experiment was done only at low temperatures. It is not clear by now how the reorientation line is located in the (H,T)-diagram relative the melting line.

X. CONCLUDING REMARKS

The nature of vortex phase transition in untwinned $YBa_2Cu_3O_{7-\delta}$ single crystals was studied by systematically varying the oxygen deficiency δ. In magnetization measurements, depending on the δ and H_{app}, the 1st order and the 2nd order phase transitions were clearly distinguished by the transition width, the magnitudes of jumps, the hysteresis in the field-cooled cooling-warming cycles and the vortex liquid undercooling. The observed inverted λ-peaks of magnetization are viewed as an admixture of a 2nd order transitory phenomenon at melting and freezing through the 1st order transition. These anomalies are observed in all the crystal orientations: $H \| a$, $H \| b$ and $H \| c$. The cooling rate dependence of the magnetization anomalies indicate that their origin is non-trivial. We suggest that their origin is linked with second order parameter (Φ-order). It was found that the order of transition changes abruptly from the 1st to the 2nd one near the optimal doping. This corresponds to moving the critical point in the (H,T)-phase diagram to $H=0$. The 1st order transition for $T>T_{CP}$, is accompanied by tiny premelting peaks in $M-H$ loops. The 2nd order transition, $T<T_{CP}$, corresponds to broad fishtails and large values of J_c. The crossover from the 1st order to the 2nd order transition at the critical point is discrete. The T and H dependencies of the magnitude of the transitory magnetization anomalies were studied along the melting lines. We point out on the lacking an adequate mean-field theoretical approach to describe these dependencies in real crystals with disorder. In addition, the 3D XY scaling approach breaks down due to the occurrence of the CP in the vortex phase diagram. The slope of the melting line changes at the CP. Therefore, the whole melting line cannot be described as a single line in which H_{c2} is suppressed by thermal fluctuations. It means that the nature of thermal fluctuation effect on the melting transition changes between the regions of the 1st order and the 2nd order transitions. The observed scaling within 3D XY model for the width of zero-field peak indicate an existence of a universal fluctuation mechanism underlying both the low-field irreversible behavior and the 1st order melting transition. Since a driving force of the scaling in the conventional XY model is a generation of vortex loops, the present results might imply that the vortex loops play an important role for both the mechanisms of melting and zero-field pinning in the high-quality crystals. The effects of the experimental artifacts on the observed 1st and 2nd order transitions are also reviewed. For the 1st order transition, a flux-flow model is suggested explaining the “non-dipolar” shape of the signal. This model is in a qualitative agreement with the observed scan-length dependencies of the SQUID response. The magnetization in the crystals with a small impurity concentration (T_c=92.5 K) are compared with those in pure high-quality untwinned crystals (T_c=93.5 K). Various factors, which contribute in changing of the nature of melting transition along the melting line, are discussed. The magnetic flux density discontinuities in a vortex system with disorder are considered along with those in a polydispersed Bernal close packing. This analysis leads to a suggestion that the magnetization jumps should decrease with increasing field along the melting line. At approaching the critical point, such a feature was indeed observed for the first time in this work.

XI REFERENCES

[1] E. Brezin, D.R. Nelson and A. Thiaville, Phys. Rev. **B31**, 7124 (1985).

[2] E. Zeldov, D. Majer, M. Konczykowski, V.B. Geshkenbein, V.M. Vinokur and H. Shtrikman, Nature **375** (1995) 373.

[3] U. Welp, J.A. Fendrich, W.K. Kwok, G.W. Crabtree and B.W. Veal, Phys. Rev. Lett. **76** (1996) 4809.

[4] R. Liang, D.A. Bonn and W.N. Hardy, Phys. Rev. Lett. **76** (1996) 835.
[5] A. Shilling, R.A. Fisher, N.E. Phillips, U. Welp, D. Dasgupta, W.K. Kwok & G.W. Crabtree, Nature **382** (1996) 792.
[6] A.I.M. Rae, E.M. Forgan and R.A. Doyle, Physica **C301** (1998) 301.
[7] J. Hu, A.H. MacDonald, Phys. Rev. **B56** (1997) 2788.
[8] M.J.W. Dodgson, V.B. Geshkenbein, H. Nordborg and G. Blatter, Phys.Rev. Lett. **80** (1998) 837.
[9] S. Ryu and D. Stroud, Phys. Rev. **B57** (1998) 14476.
[10] D.S. Fisher, M.P.A. Fisher and D.A. Huse, Phys. Rev. **B43,** (1991) 130.
[11] H. Safar, P.L. Gammel, D.A. Huse, D.J. Bishop, W.C. Lee, J. Giapintzakis and D.M. Ginsberg, Phys. Rev. Lett. **70**, (1993) 3800.
[12] D. Lopez, L. Krusin-Elbaum, H. Safar, E. Righi, F. de la Cruz, S. Grigera, C. Feild, W.K. Kwok, L. Paulius, G.W. Crabtree, Phys. Rev. Lett. **80**, (1998) 1070.
[13] A.I. Rykov, Physica (Amsterdam) C**297** (1998) 133.
[14] A.I. Rykov, S. Tajima, F.V. Kusmartsev, E.M. Forgan and Ch. Simon, Phys. Rev.**B60** (1999) September 1.
[15] T.B. Lindemer, J.F. Hunley, J.E. Gates, A.L. Sutton, J. Brynestad, C.R. Hubbard, J.Am. Ceram. Soc. **72**, (1989) 1775.
[16] N.D. Antunes, L.M.A. Bettencourt and W.H. Zurek, Phys. Rev. Lett. **82** (1999) 2824.
[17] Z. Tesanovic, Phys. Rev. **B59** (1999) 6449.
[18] C. Bäuerle, Yu.M. Bunkov, S.N. Fisher, H. Godfrin and G.R. Pickett, Nature, **382** (1995) 332.
[19] V.M.H. Ruutu, V.B. Eltsov, A.J. Gill, T.W.B. Kibble, M. Krusius, Yu.G. Makhlin, B. Plaçais, G.E. Volovik and Wen Xu, Nature, **382** (1996) 334.
[20] N.D. Antunes and L.M.A. Bettencourt, Phys. Rev. Lett. **81** (1999) 3083.
[21] C.P. Bean, Rev.Mod.Phys. **36**(1964)31.
[22] J.R. Cooper, J.W. Loram, J.D. Johnson, J. W. Hodby, C. Changkang, Phys. Rev. Lett. **79**, 1730 (1997).
[23] T. Giamarchi and P. Le Doussal, Phys. Rev. **B55** (1997)6577.
[24] D. Ertaš and D.R. Nelson, Physica C.272 (1996) 79.
[25] T. Nishizaki, T. Naito and N. Kobayashi, Phys. Rev. **B58** (1998) 11169.
[26] S.S. Banerjee, N.G. Patil, S. Saha, S. Ramakrishnan, A.K. Grover, S. Bhattacharya, G. Ravikumar, P.K. Mishra, T.V. Chandrasekhar Rao, V.C. Sahni, M.J. Higgins, E. Yamamoto, Y. Haga, M. Hedo, Y. Inada, Y. Onuki, Phys. Rev. **B58** (1998) 995.
[27] X.S. Ling, J.E. Berger, D.E. Prober, Phys. Rev. **B57** (1998) R3249.
[28] G. Ravikumar, T.V. Chanrasekhar Rao, P.K. Mishra, V.C. Sahni, S.S. Banerjee, A.K. Grover, S. Ramakrishnan, S. Bhattacharya, M.J. Higgins, E. Yamamoto, Y. Haga, M. Hedo, Y. Inada, Y. Onuki, Physica **C298** (1998)122.
[29] G. Ravikumar, T.V. Chanrasekhar Rao, P.K. Mishra, V.C. Sahni, Subir Saha, S.S. Banerjee, N.G. Patil, A.K. Grover, S. Ramakrishnan, S. Bhattacharya, M.J. Higgins, E. Yamamoto, Y. Haga, M. Hedo, Y. Inada, Y. Onuki, Physica **C276** (1997)9.
[30] W.K. Kwok, J.A. Fendrich, C.J. van der Beek, G.W. Crabtree, Phys.Rev.Lett. **73** (1994) 2614.
[31] M. Willemin, A. Shilling, H. Keller, C. Rossel, J. Hofer, U. Welp, W.K. Kwok, R.J. Olsson and G.W. Crabtree, Phys. Rev. Lett. **81** (1998) 4236.
[32] D.E. Farrell, E. Johnston-Halperin, L. Klein, P. Fournier, A. Kapitulnik, E.M. Forgan, A.I.M.Rae, T.W. Li, M.L. Trawick, R. Sasik, J.C, Garland, Phys.Rev. **B 53** (1996) 11807.
[33] M. Willemin, C. Rossel, J. Hofer, H. Keller, A. Erb and E. Walker, Phys. Rev. **B58** (1998)R5940.

[34] G. Blatter, M.V. Feigel'man, V.B. Geshkenbein, A.I. Larkin and V.M. Vinokur, Rev. Mod. Phys. **66** (1994) 1125.
[35] X. Hu, S. Miyashita, M. Tachiki, Phys. Rev. **B58** (1998)3438
[36] A.E. Koshelev and H. Nordborg, Phys. Rev. **B59** (1999)4358.
[37] K. Deligiannis, P.A.J. de Groot, M. Oussena, S. Pinfold, R. Langan, R. Cagnon and L. Taillefer, Phys. Rev. Lett. **79** (1997) 2121.
[38] H. Küpfer, Th. Wolf, C. Lessing, A.A. Zhukov, X. Lançon, R. Meier-Hirmer, W. Schauer, and H. Wühl, Phys. Rev. B58 (1998) 2886.
[39] H. Zheng, M. Jiang, B.W. Veal, H. Claus, B. Obst, Physica **C301** (1998) 147.
[40] A. Junod, M. Roulin, J.-Y. Genoud, B. Revaz, A.Erb, and E. Walker, Physica (Amsterdam) **275C** (1997) 245.
[41] M.B. Salamon, J. Shi, N. Overend, M.A. Howson, Phys. Rev. **B 47** (1993) 5520.
[42] A.I. Rykov, W.J. Jang, H. Unoki, S. Tajima, in *Advances in Superconductivity VIII*, edited by H. Hayakava and Y. Enomoto (Springer-Verlag, Tokyo, 1996) p. 341.
[43] M.J.W. Dodgson, V.B. Geshkenbein, H. Nordborg and G. Blatter, Phys.Rev. B**57** (1998) 14498.
[44] M. A. Hubbard, M.B. Salamon, B.W. Veal. Physica (Amsterdam) **259C** (1996) 309.
[45] S. Kamal, D.A. Bonn, N. Goldenfeld, P.J. Hirschfeld, R. Liang and W.H. Hardy, Phys. Rev. Lett. **73** (1994) 1845.
[46] T. Sasagawa, K. Kishio, Y. Togawa, J. Shimoyama and K. Kiytazawa, Phys. Rev. Lett. **80** (1998) 4297.
[47] A. Shilling, R.A. Fisher, N.E. Phillips, U. Welp. W.K. Kwok, and G.W. Crabtree, Phys. Rev. **B58** (1998) 11157.
[48] X.G. Qui, V.V. Moshchalkov, Y. Bruynseraede, and J. Karpinski, Phys. Rev. **B58** (1998) 8826.
[49] M. McElfresh, S. Li, R. Sager. Technical Advisory, Quantum Design (1996).
[50] V.B. Geshkenbein, L.B. Ioffe, A.I. Larkin, Physica **A**(1993)278.
[51] V.B. Geshkenbein, L.B. Ioffe, A.I. Larkin, Phys.Rev.**B48**(1993)9917.
[52] A. Zieba, Rev. Sci. Instrum. **64**(1993)3357.
[53] C.N. Guy, J.O. Strom-Olsen, R.W. Cochrane, Phys. Rev.Lett. **42**(1979)257.
[54] C. N. Guy, W. Howarth, J.Phys. **C11** (1978)1635.
[55] C.N. Guy, J. Phys. **F.12**(1982)1453.
[56] R. Kumar, A.K. Grover, P. Chaddah, C.K. Subramanian, V. Sankaranavaryanan, Sol. St. Comm. **76** (1990) 175.
[57] A. K. Grover, R. Kumar, S.K. Malik, P. Chaddah, Sol. St. Comm. **77** (1991) 723.
[58] M. Suenaga, D.O. Welch, R. Budhani, Supercond. Sci. Technol. **5** (1992) Suppl., pp.1-8.
[59] A.A. Zhukov, V.V. Moshchalkov, V.D. Kuznetsov, V.V. Metlushko, G.T. Karapetrov, E.V. Pechen, and V.I. Timashev, Sov. Phys. JETP **73** (1991)334.
[60] L.L. Miller, Rev. Sci. Instrum.**67**(1996) 3201.
[61] S. Libbrecht, E. Osquiguil, and Y. Bruynseraede, Physica **C 225** (1996) 337.
[62] M. Suzuki, K. Miyahara, S. Kubo, S. Karimoto, K. Tsuru, and K. Tanabe, in Advances in Superconductivity VII, ed. by K. Yamafuji, T. Morishita(Springer-Verlag, Tokyo, 1995) pp.213-217.
[63] A. Wienss, G. Jakob, P. Voss-de Haan, and H. Adrian. Physica **C 280** (1997)158.
[64] F.J. Blunt, A.R. Perry, A.M. Campbell, and R.S. Liu, Physica **C 175** (1991)539.
[65] S.B. Roy, A.K. Pradhan, P. Chaddah, Physica **C271** (1996) 181.
[66] A.I. Rykov and S. Tajima, In: Advances in Superconductivity IX, Eds. Murakami M. and Nakajima S. (Tokyo: Springer-Verlag, 1997) 503.
[67] A.I. Rykov, S. Tajima and F.V. Kusmartsev, Int. J. Mod. Phys. **12** (1998) 3326.

[68] G.A. Williams, Phys. Rev. Lett. **82** (1999)1201.
[69] M. Friesen, P. Muzikar, Physica **C302** (1998) 67.
[70] C.M. Aegerter, S.T. Johnson, W.J. Nuttall, S.H. Lloyd, M.T. Wylie, M.P. Nutley, E.M. Forgan, R. Cubitt, S.L. Lee, D. McK. Paul, M. Yethiraj and H.A. Mook, Phys. Rev. **B57** (1998) 14511.
[71] M. Roulin, A. Junod, A. Erb, and E. Walker, Phys. Rev. Lett. **80** (1998) 1722.
[72] M. Roulin, A. Junod, and E. Walker, Physica **C 296** (1998) 137.
[73] B. Revaz, A. Junod, and A. Erb, Phys. Rev. **B58** (1998) 11153.
[74] R.M. Langan, S.N. Gordeev, P.A.G. de Groot, A.G.M. Jansen, R. Gagnon, and L. Taillefer, Phys. Rev. **B58** (1998) 14548.
[75] S.E. Phan, W.B. Russel, J.Z. Zhu and P.M. Chaikin, J. Chem. Phys. **108** (1998) 9789.
[76] P. Bartlett, J. Chem. Phys. **107** (1997) 188.
[77] P. Barlett, P.B. Warren, Phys. Rev. Lett. **82** (1999)1979.
[78] S.T. Johnson, E.M. Forgan, S.H. Lloyd, C.M. Aegerter, S.L. Lee, R. Cubitt, P.G. Kealey, C. Ager, S. Tajima, A.I. Rykov, D. McK. Paul, Phys. Rev. Lett. **82**(1998) 2792.